

Medizinische Fakultät der Charité – Universitätsmedizin Berlin Campus
Benjamin Franklin

aus der Klinik für Kardiologie / Innere Medizin

Deutsches Herzzentrum Berlin

Abteilungsleiter: Professor Dr. Eckart Fleck

In vitro Characterization of Magnetic Resonance Imaging Contrast Agents for Molecular Imaging

Inaugural-Dissertation

zur Erlangung der
medizinischen Doktorwürde

der Charité – Universitätsmedizin Berlin

Campus Benjamin Franklin

Vorgelegt von

Zhi Yu

Aus Yunnan, V. R. China

Referent: Professor Dr. Eckart Fleck

Koreferent:

Gedruckt mit Genehmigung der Charité – Universitätsmedizin Berlin
Campus Benjamin Franklin

Promoviert am: 5.9.2006

**Für meinen Gatten Hang He und
meinen Sohn Zhi-feng He**

CONTENTS

1	INTRODUCTION	1
2	MATERIALS AND METHODS	3
2.1	CELL CULTURE	3
2.1.1	<i>Human umbilical vein endothelial cells</i>	3
2.1.1.1	Cell culture condition	3
2.1.1.2	Isolation of human umbilical vein endothelial cells	4
2.1.2	<i>Mouse endothelial cell line</i>	4
2.1.3	<i>THP-1 cells</i>	4
2.1.3.1	Staining of THP-1 cells	5
2.1.4	<i>Isolation of mouse splenocytes</i>	5
2.2	IRON OXIDE PARTICLES	6
2.2.1	<i>Preparation of magnetically labeled monoclonal antibodies</i>	7
2.3	MEASUREMENT OF NANOPARTICLE UPTAKE IN CELL CULTURE	7
2.3.1	<i>Histochemistry: Prussian blue staining</i>	7
2.3.2	<i>Measurement of iron uptake by endothelial cells and THP-1 cells</i>	8
2.3.2.1	Incubation	8
2.3.2.2	Pretreatment with inhibitors of endocytosis	9
2.3.2.3	Iron measurement	9
2.4	SPECIFIC BINDING OF NANOPARTICLES TO CELLS	11
2.4.1	<i>Flow cytometry</i>	11
2.4.2	<i>Antibodies</i>	12
2.5	STATISTICS	13
3	RESULTS	14
3.1	HISTOCHEMISTRY: PRUSSIAN BLUE	14
3.2	MEASUREMENT OF IRON UPTAKE	18
3.2.1	<i>Effect of endocytosis inhibitors</i>	24
3.3	FLOW CYTOMETRY MEASUREMENT	26
4	DISCUSSION	31
4.1	DISCUSSION OF METHODS	31
4.1.1	<i>Why was CD40 and CD62E monoclonal antibody chosen for specific labeling?</i>	31
4.1.2	<i>Why were human umbilical vein endothelial cells, the mouse endothelial cell line bEnd.3 und human macrophages chosen for measurement of unspecific uptake of nanoparticles?</i>	33
4.1.3	<i>Rationale for the iron concentrations of nanoparticles used</i>	34
4.2	CHARACTERIZATION OF IRON OXIDE PARTICLES	35
4.2.1	<i>Unspecific uptake</i>	35
4.2.2	<i>Uptake inhibited by colchicine and cytochalasin B</i>	37
4.2.3	<i>Specific binding of antibody-CLIO conjugate</i>	39
5	SUMMARY	45
6	ABBREVIATIONS	46
7	REFERENCES	47
8	ANHANG	54
8.1	DANKSAGUNG	54
8.2	EIDESSTÄTTLICHE ERKLÄRUNG	55
8.3	LEBENS LAUF	56

1 Introduction

Molecular imaging is a non-invasive and repetitive means of imaging targeted macromolecules and biological processes in living organisms (¹). It has the potential to provide three-dimensional information much faster than is currently possible with conventional time-consuming, labor-intensive, invasive techniques such as histologic analysis.

A major aim of molecular imaging today is to achieve high specificity and to improve sensitivity. Whereas conventional MRI methods do not provide the necessary sensitivity and contrast for imaging at the cellular level, new techniques are emerging for imaging of biochemical processes and cellular events using magnetic resonance imaging (MRI) by labeling individual cells with paramagnetic compounds to achieve signal amplification and improve sensitivity(^{2;3}).

Several laboratories have investigated the feasibility of using MRI to visualize monocytes and lymphocytes. Nanometer-sized superparamagnetic iron oxide particles (SPIO) comprising magnetite ($\text{FeO}\cdot\text{Fe}_2\text{O}_3$) coated with citrate or dextran were used for these tests. Other studies (^{4;5}) demonstrated that in animal models, i.v. injected SPIO particles with significant inflammatory responses are internalized by monocytes and can be detected using MRI at the sites of inflammation (⁶⁻⁸).

These studies demonstrated that SPIO particles with a modified surface can be used for molecular imaging, such as receptor-directed imaging, cell labeling for in-vivo monitoring of cell migration, e.g., stem cell labeling, and labeling of gene constructs for localization in genetic therapy.

Superparamagnetic iron oxide (SPIO) particles can be manufactured with different particle sizes and surface coatings. The particles investigated so far differ markedly in their pharmacokinetic properties, cell specificity, and effects on MR signal intensity

caused by differences in size and chemical modification.

Large SPIO particles (50-150 nm) predominantly produce a signal decrease or T2-shortening and have been used as contrast media for MRI of the liver and spleen. Smaller particles (about 20 nm in diameter) show a different organ distribution and have a potential for improving noninvasive lymph node assessment or characterizing vulnerable atherosclerotic plaques (⁹). The prototype of smaller SPIO was developed by Weissleder et al. The hydrodynamic diameter is 11.4 ± 6.3 nm and the blood half-life of the T1 effects is 80 minutes (¹⁰). The small size and prolongation of blood half-life enable this agent to cross the capillary wall and achieve more widespread tissue distribution, leading to extensive uptake by targeted cells.

Nanoparticle coatings may be comprised of several materials including both inorganic and polymeric materials(¹¹). Polymeric coating materials can be classified into synthetic and natural, including use of dextran, gelatin, chitosan and pullulan (^{12;13}).

Special surface coating of the SPIO particles has to be non-toxic and biocompatible but must also allow targetable delivery with particle localization in a specific area (¹⁴).

Objective

The aim of this work was to evaluate the biological properties of three paramagnetic particles with comparable size but different surface coating. One particle was coated with dextran, the second particle was coated with cross-linked dextran and the third was coated with citrate. The unspecific uptake of both particles by human endothelial cells, murine endothelial cells and human macrophages was examined by measurement of cellular iron content. Furthermore the effect of known inhibitors of endocytosis shall be evaluated. In addition, it was studied whether linking of monoclonal antibodies to dextran coated particles can make them bind specifically to certain cell surface structures.

2 Materials and methods

2.1 Cell culture

2.1.1 Human umbilical vein endothelial cells

2.1.1.1 Cell culture condition

Human umbilical vein endothelial cells (HUVEC) were cultured in medium 199 containing 20% fetal calf serum (GIBCO, Germany), 1% L-glutamin (200 mM), 1% penicillin (100 U/ml) and 1% streptomycin (100 µg/ml), 1% amphotericin (250 µg/ml), 10 mmol/L Hydroxyethylpiperazine-ethane sulfonic acid (HEPES) buffer (Sigma, Germany), and 10 ng/ml endothelial cell growth factor- α (α FGF, Pepro Tech, Inc, Britain) in a 5% CO₂ incubator at 100% humidity and 37°C. Before use, the culture flasks were coated with gelatin by incubation for at least 24 hours at 4°C with 0.2% gelatin (Sigma, Germany). The cells were regularly monitored using an inverted light microscope and culture medium was changed three times a week.

When the cultures reached confluency they were subcultured at a split ratio of 1:3. The culture medium was removed and the cultures were rinsed 3 times with PBS without Ca²⁺ and Mg²⁺ to remove all traces of serum which contains trypsin inhibitors. Then, 2.5ml of 0.25%-Trypsin/0.02%-Ethylenediaminetetraacetic acid (EDTA) solution was added to the culture flasks and incubated for 3 minutes at 37°C and the detachment of the cells was monitored under an inverted microscope (Zeiss, Germany). Upon complete detachment of the cells, 5.0ml of complete culture medium was added and the cells were collected in a 50 ml Falcon tube. The cells were pelleted by centrifugation at 200g for 5 minutes. The supernatant was discarded and the cell pellet was resuspended by pipette or vortex with fresh culture medium and transferred into new culture flasks.

2.1.1.2 Isolation of human umbilical vein endothelial cells

Endothelial cells from human umbilical veins were isolated according to a protocol by Jaffe et al. (¹⁵) which was slightly modified (^{16;17}). The umbilical cord was clamped shut immediately after birth and placed in PBS with Ca/Mg, penicillin (100 U/ml)/streptomycin (100µg/ml). The cord was inspected, and all areas of the cord with clamp marks were cut off. A cord has one vein and two arteries. Usually, the vein has a larger diameter and a more flexible wall than the arteries. The umbilical vein was cannulated with a sterile i.v. cannula. The cannula was fixed and the vein was perfused with phosphate buffered saline (PBS) (without Ca/Mg) using a 20ml syringe to wash the blood out. 10 ml Dispase-II solution (Boehringer-Mannheim, Germany) was then infused into the umbilical vein, and the cord was incubated at 37°C for 30 min. After incubation, the Dispase-II solution containing the endothelial cells was flushed from the cord vein by perfusion with 20 ml complete medium. The effluent was collected in a sterile 50 ml centrifuge tube (Falcon, USA). The cells were sedimented at 200g for 5 minutes. The cell pellet was resuspended in fresh culture medium and grown in gelatin-coated 75cm² flasks.

2.1.2 Mouse endothelial cell line

A mouse endothelial cell line (bEnd.3) was obtained from the American Type Culture Collection (ATCC, USA) and cultured in Dulbecco's modified Eagle's medium (DMEM) containing 10% fetal bovine serum (GIBCO, Germany), 0.5% Gentamycin (10mg/ml), 1% amphotericin (250µg/ml), 10 mmol/L HEPES buffer (Sigma, Germany) at 37°C in 100% humidity. The subculture procedure is the same as for HUVEC, but the culture flasks need no gelatin coating.

2.1.3 THP-1 cells

The human pre-monocytic cell line (THP-1) (ATCC) was propagated in Roswell Park

Memorial Institute (RPMI) 1640 medium containing 10% fetal calf serum (GIBCO, Germany), 1% penicillin (100U/ml) and 1% streptomycin (100µg/ml) at 37°C in 5% CO₂. Every 3 to 5 days cells were diluted to 0.1-1.0×10⁶ cells/ml.

2.1.3.1 Staining of THP-1 cells

To monitor the differentiation, THP-1/macrophages were allowed to adhere to gelatin-coated (0.2%) plastic chamber slides and then fixed with 4% buffered methanol for 20 minutes at room temperature. Non-specific binding was blocked with 10% normal-goat serum, followed by washing with PBS/0.01% Triton-X100 several times. Primary antibodies (all diluted 1:50) were incubated overnight at 4°C. After washing with PBS/0.01% Triton-X100 several times, fluorescein isothiocyanate (FITC)- or Avidin D-Texas Red (TXR)-conjugated secondary antibodies were used (Vector). Specificity controls were done by omission of the first antibody and/or incubation with non-immune IgGs.

2.1.4 Isolation of mouse splenocytes

Murine spleen cells contain about 50% B-lymphocytes and were used as a test system for CD40 antibody and VSOP CD40 antibody constructs.

A mouse spleen was mechanically dissociated on a 250µm metallic strainer, washed in 50 ml PBS, and filtered through a 70-µm cell disposable strainer (Becton Dickinson Labware, Bedford, MA, USA). The cell suspension was then centrifuged at 400g for 8 minutes, and the pellet was resuspended in 10ml cold PBS.

2.2 Iron oxide particles

Table 1: Characterization of iron oxide particles used

Name	VSOP (very small superparamagnetic iron oxide particles)	CMD-coated particles	CLIO (cross-linked iron oxide particles)
Origin (contact)	Ferropharm GmbH; Teltow, Germany (PD Dr. M. Taupitz)	Berlin Heart AG; Berlin, Germany (Dr. N. Buske)	Center for Molecular Imaging Res. Harvard Med. School Charlestown, MA, U.S.A. (Prof. R. Weissleder)
Coat	citrate	carboxymethyl-dextran (CMD)	dextran
Coat crosslinking (stabilizing the coat)	no	no	yes
Functional groups at the coat	-COOH	-COOH	-NH ₂
Core diameter (only iron oxide core; transmission electron microscopy)	4nm	ca. 10nm	3 – 5nm
Hydrodynamic diameter (with coat; laser light scattering)	8.6nm	150 – 200nm	30 – 40nm

2.2.1 Preparation of magnetically labeled monoclonal antibodies

The preparation of magnetically labeled monoclonal antibodies (mabs) is based on earlier work in cooperation with Prof. Weissleder. CLIOs (cross-linked iron oxide) (generous gift from R. Weissleder) are superparamagnetics consisting of an iron oxide core and covered by a cross-linked dextran coat bearing free amino groups (NH₂-groups). Using suberic acid monoNHS ester, suberic acid was coupled to the amino groups resulting in carboxylated particles. These particles were then conjugated to monoclonal antibodies of choice with the aid of the EDC/NHS method. Using fluorescence labeled antibodies or by subsequent reaction with NHS ester of fluorescence markers, a second label can be introduced (¹⁸). CLIO-antibody constructs were prepared in our laboratory and provided for testing.

2.3 Measurement of nanoparticle uptake in cell culture

2.3.1 Histochemistry: Prussian blue staining

Human umbilical vein endothelial cells (HUVEC) and murine bEnd.3 cells were plated at an initial density of 20,000 cells/well onto 0.1% gelatin-coated 8-well chamber slides. Cells were allowed to reach confluence, which was observed to happen usually within 48 hours. Cells were incubated with the different paramagnetic particles that were serially diluted in culture medium at 37°C. At 30 minutes, 2 hours, 8 hours and 24 hours following addition of the particles, the cells were carefully washed three times with cold PBS (with Ca/Mg, pH 7.4) to remove unbound particles. The upper structure and gasket of the chamber were removed, and the cells fixed with 100% Methanol (-20°C). Each experiment was performed in triplicate.

To demonstrate the uptake of the different paramagnetic particles by endothelial cells, the slides were stained with Prussian blue. The reaction occurs when the sections

are treated in acid solutions of ferrocyanides. Any ferric ion (+3) combines with the ferrocyanide and results in the formation of a bright blue pigment called “Prussian blue” or “Berliner Blau”.

Slides were rinsed in distilled water, incubated with freshly prepared potassium ferrocyanide (2%) : hydrochloric acid (2%) = 1:1, rinsed again in distilled water, and counter stained with nuclear-fast red (Sigma-Aldrich Chemie GmbH, Steinheim, Germany) for 30 minutes and washed with tap water. A coverslip with Kaiser's glycerol gelatine (Merck, Darmstadt, Germany) was placed on top.

2.3.2 Measurement of iron uptake by endothelial cells and THP-1 cells

2.3.2.1 Incubation

HUVECs and murine bEnd.3 cells were plated at an initial density of 50,000 cells/well onto a 0.1% gelatin-coated 24-well plate. Cells were allowed to reach confluence which was observed to happen usually within 48 hours.

THP-1 (5×10^4 cells/well) were plated at an initial density of 50,000 cells/well onto a 24-well plate, and incubated for 48 hours with 10 nM phorbol 12-myristate 13-acetate (PMA), which induces differentiation of THP-1 cells to macrophages (^{19;20}).

Confluent HUVECs and bEnd.3 cells as well as THP-1/macrophages were incubated with the different paramagnetic particles that were serially diluted in culture medium at 37°C. At 30 minutes, 2 hours, 8 hours and 24 hours the cells were carefully washed three times with PBS (with Ca/Mg, pH 7.4) to remove unbound particles. Then cells were dissolved in 100µl 0.1% sodium dodecyl sulfate (SDS). The samples from each well were transferred to microcentrifuge tubes. Each experiment was performed in triplicate.

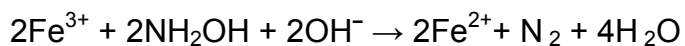
2.3.2.2 Pretreatment with inhibitors of endocytosis

The uptake mechanism of particles was investigated by supplementing the medium with 50 µg/ml colchicine (Sigma Aldrich Chemie GmbH, Germany) or 5 µg/ml cytochalasin B (Sigma Aldrich Chemie GmbH, Germany) for 4 hours. Before addition of the paramagnetic particles, the cells were washed twice in PBS.

2.3.2.3 Iron measurement

The reaction between ferrous ions and 1,10-phenanthroline forming a red complex, which is measured at 508 nm $\text{Fe}(\text{phen})_3^{2+}$, is a sensitive method for determining iron concentrations. The intensity of the color does not change appreciably over 3 hours. The pH has to be adjusted to a value of between 6 and 9 (not under 6.0!). This method is twice as sensitive as the Rhodanid method (Fe^{3+} : SCN; 474nm) and 20-200 times more sensitive than determination of iron by measuring the absorbance of Fe^{3+} at 410 nm (see Truman State University CHEM 222 Lab Manual).

Hydroxylamine can be used to reduce any ferric ions that are present:



A standard solution was prepared from pure ferrous ammonium sulfate hexahydrate $\text{Fe}_2(\text{NH}_4)_2(\text{SO}_4)_2 \cdot 6\text{H}_2\text{O}$ dissolved in water and sulfuric acid.

Table 2: Standard solution preparation

Standard μl	Water μl	Hydroxy- lamine μl	Phenanthroline μl	Na- acetate μl	Fe ²⁺ ng/ml /factor
0 (blank)	500	10	100	390	0
10	490	10	100	390	99.7/100
50	450	10	100	390	498.5/20
100	400	10	100	390	997.0/10
250	250	10	100	390	2492.5/4
500	0	10	100	390	4985.0/2

30 μl of the particle suspension and 25 μl 6N HCL were incubated in Eppendorf tubes for 10 minutes at 100°C with occasional vortexing. Then 795μl sodium acetate solution was added; 750 μl of this solution was mixed with 585 μl Na-acetate (100mg/ml) and 150 μl phenanthroline (1 mg/ml) + 15 μl hydroxylamine hydrochloride (10 mg/ml).

Absorbance was measured at 490nm in an ELISA reader and concentrations were calculated using the standard curve. Data were defined as the residual values between means of the uptake and binding experiments for each time point.

2.4 Specific binding of nanoparticles to cells

2.4.1 Flow cytometry

Flow cytometry of endothelial cells and THP-1 cells was performed to estimate cell surface expression of CD40, E-selectin and CD31.

Endothelial cells were seeded onto 60-cm² culture dishes and grown to confluence. Next, some of the cultures were activated with 500 IU/ml murine tumor necrosis factor (mTNF)- α or human TNF- α for 0.5, 2, 4, 8 hours, respectively.

Following activation, endothelial cells were scraped off the culture dish with a “rubber policeman”. Approximately 2×10^5 cells were incubated with the primary antibody-CLIO complexes, as described in section 2.2.1, CLIO rat anti-mouse CD62E (γ IgG2a) (antibody of clone 10E9, Prof. Dietmar Vestweber, Münster) or CLIO rat IgG2a (isotype control) for 30 minutes on ice. The cells were washed three times with PBS and were then incubated with a FITC-labeled mouse or goat anti-ratIgG secondary antibody at 15 μ g/100 μ l for 30 minutes on ice in the dark. In contrast, cells were stained with rat anti-mouse CD62-PE or isotype control rat IgG2a-PE in PBS-BSA-hIgG azide. As a negative cell control, unstimulated endothelial cells were incubated in analogous experiments.

Freshly prepared mouse splenocytes as described in cell culture (2.1.4) were labeled for 30 minutes on ice with rat anti-mouse CD40 (clone FGK, Prof. Roling, Basel) of its CLIO conjugate or CLIO rat IgG2a conjugate as isotype control and then with a secondary antibody Goat-F(ab')-anti-rat IgG(H+L)-FITC. By comparison, spleen cells were labeled with anti-mouse CD40-PE or isotype control rat IgG2a-PE.

The fluorescence of the cells was measured with a Fluorescence Activated Cell Scanner (BD Biosciences, Heidelberg, Germany). Data were further analyzed using

CELLQuest software (San Jose, CA). Generation of the fluorescence histograms and calculation of median and mean fluorescence values of the different populations was done using the WinMDI 2.8 software (<http://facs.scripps.edu/facsindex.html>) after gating.

2.4.2 Antibodies

The antibodies used to test specific binding of paramagnetic particles are summarized in table 3.

Table 3: Primary antibodies and secondary antibodies used for FACS experiments

Primary antibody		Secondary antibody	
Rat anti-mouse CD31 (rIgG2a kappa); BD Pharmingen (Heideberg, Germany)	0.5mg/ml; 2.5µg/ 100µl	Mouse anti-rat IgG (H+L)-FITC; Jackson-Immuno Research (Pennsylvania,USA)	1.25mg/ml; 6.7µl/100µl
Rat anti-mouse CD40PE BD Pharmingen (Heideberg, Germany)	0.8µg/100µl		
Anti-mouse CD62-PE (E-selectin ELAM-1); BD Pharmingen (Heideberg, Germany)	0.8µg/100µl		
Rat anti-mouseCD62E(rIgG2a) (clon 10E9, Prof. Dietmar Vestweber, Münster)	50µg/100µl	Goat anti-rat IgG(H+L)-FITC; Jackson Immuno Research (Pennsylvania, USA)	1.5mg/ml; 15µg/ 100µl
		Mouse anti-rat IgG(H+L)-FITC; Jackson Immuno Research (Pennsylvania, USA)	1.25mg/ml ; 10µl/100µl
antiCD40 (clone FGK, Prof. Roling, Basel)			
RatIgG2a (isotype-PE); BD Pharmingen (Heideberg, Germany)	2.5µg; 5µg/100µl		

2.5 Statistics

Results are shown as means \pm standard deviation (SD); n is the number of experiments. Cell numbers were separately counted in each experiment. For statistical evaluation, the effect of particle surface coating and the influence of endocytic inhibitors on cellular iron uptake were compared using the Student t test. P-values < 0.05 were considered significant.

The mean represents a measure of central tendency for a distribution. Median is the value above and below which 50% is distributed. In a symmetrical distribution, the mean is equal to the median. In a skewed distribution, the mean and median have different values.

3 Results

3.1 Histochemistry: Prussian blue

Endothelial cells from human umbilical veins and the bEnd.3 cell line, which has been described as a model for murine endothelial cells, were examined for paramagnetic iron particle uptake by histochemistry. Light microscopy in conjunction with Prussian blue staining was used to characterize the internalized paramagnetic particles as well as a calorimetric iron assay.

The internalized paramagnetic particles react with the ferrocyanides and this results in the formation of a bright blue pigment called “Prussian blue” or “Berliner Blau”. Nuclei are red and the background is pink. The histochemistry results show that nanoparticle uptake was dependent on the incubation time and particle concentration. The uptake was seen as early as at 30 min and increased gradually with incubation time (Fig. 1 from left to right).

The different nanoparticles were used at concentrations ranging from 27 μ g Fe/ml to 217.5 μ g Fe/ml. At a concentration of 217.5 μ g Fe/ml, more dark blue pigments are visible than at the lower concentrations. The representative micrographs of Prussian blue staining of bEnd.3 monolayers for two different particles (VOSP-C184 and CMD) are given in Figure 1 (A-D) at concentrations of 217.5 μ g Fe/ml and 108.8 μ g Fe/ml. Comparison of the same nanoparticle showed that uptake was dependent on iron concentration in the medium.

The uptake of citrate-coated nanoparticles (VSOP) was already observed 30 minutes after starting the incubation, and it increased rapidly during the next 2 to 8 hours. At the same time point (0.5, 2h), there were few blue granules of carboxydextran-coated nanoparticles (CMD) in cells. While the uptake of both particles after 24h incubation was clearly visible, the staining was considerably less intense.

The results in HUVEC given in Fig. 1 (E-H) are comparable to those derived from bEnd.3 cells. However, at the highest iron concentration of 217.5 μ g Fe/ml HUVEC, more cells detached from the culture dish after 24 hours incubation than with bEnd.3 cells.

Importantly, CLIO also showed cellular uptake, but to a lesser degree than other nanoparticles tested (Fig. 2).

It was observed that:

- 1) The cellular uptake of citrate-coated nanoparticles (VSOP) is significantly higher than that of the dextran-coated nanoparticles.
- 2) Uptake is higher for murine endothelial cells (bEnd.3), which are known to have higher proliferating activity than human endothelial cells (HUVEC).
- 3) The blue pigments are localized mostly in the cytoplasm.

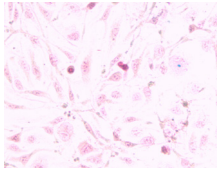
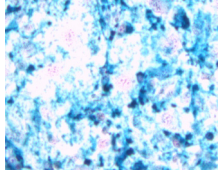
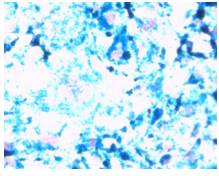
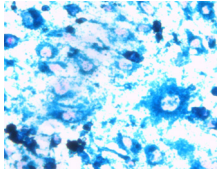
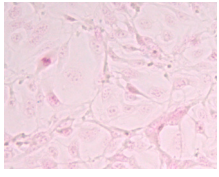
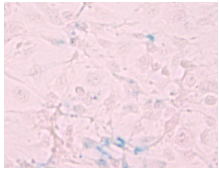
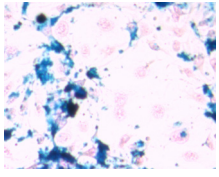
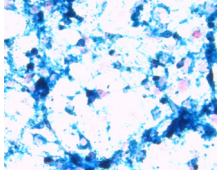
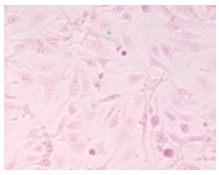
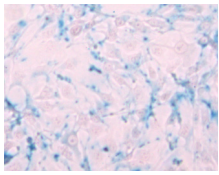
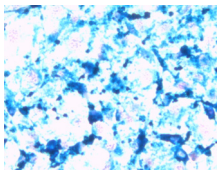
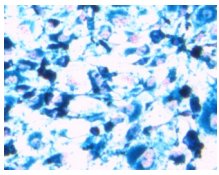
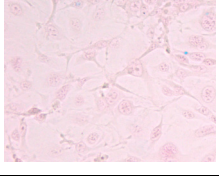
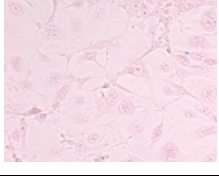
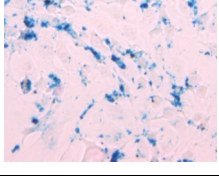
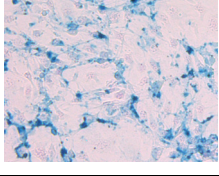
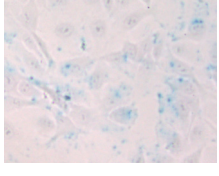
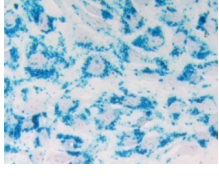
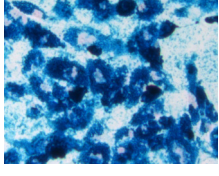
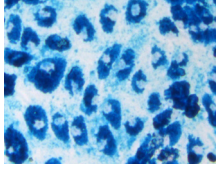
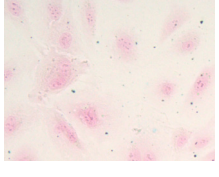
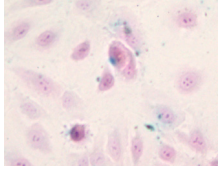
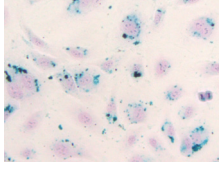
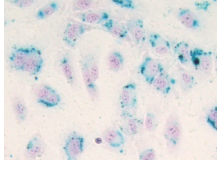
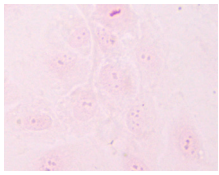
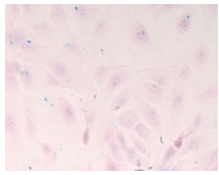
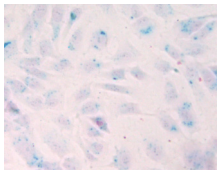
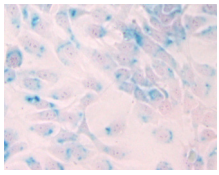
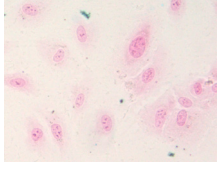
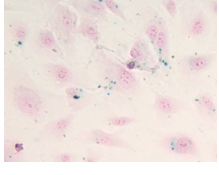
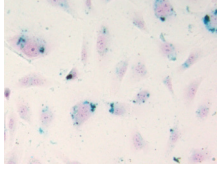
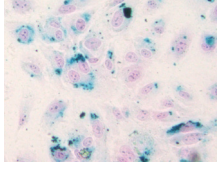
	0.5h	2h	8h	24h	
bEnd.3 VSOP 0.2175 mg/ml					A
bEnd.3 CMD 0.2175 mg/ml					B
bEnd.3 VSOP 0.1088 mg/ml					C
bEnd.3 CMD 0.1088 mg/ml					D
HUVEC VSOP 0.2175 mg/ml					E
HUVEC CMD 0.2175 mg/ml					F
HUVEC VSOP 0.1088 mg/ml					G
HUVEC CMD 0.1088 mg/ml					H
	1	2	3	4	

Figure 1: Micrographs of bEnd.3 monolayers (A, B, C, D) and human umbilical vein endothelial cell monolayers (E, F, G, H) incubated with the citrate-coated (VSOP) and carboxydextran-coated (CMD) paramagnetic particles. Blue precipitate within the cells represents internalized iron particles. Stained cells are shown after 30 minutes (A1-H1), 2 hours (A2-H2), 8 hours (A3-G3) and 24 hours (A4-G4) of incubation with paramagnetic particles of two different concentrations (0.2175mg Fe/ml and 0.1088mg Fe/ml). Note increasing intracellular iron uptake with higher concentrations of iron oxide in the incubation medium.

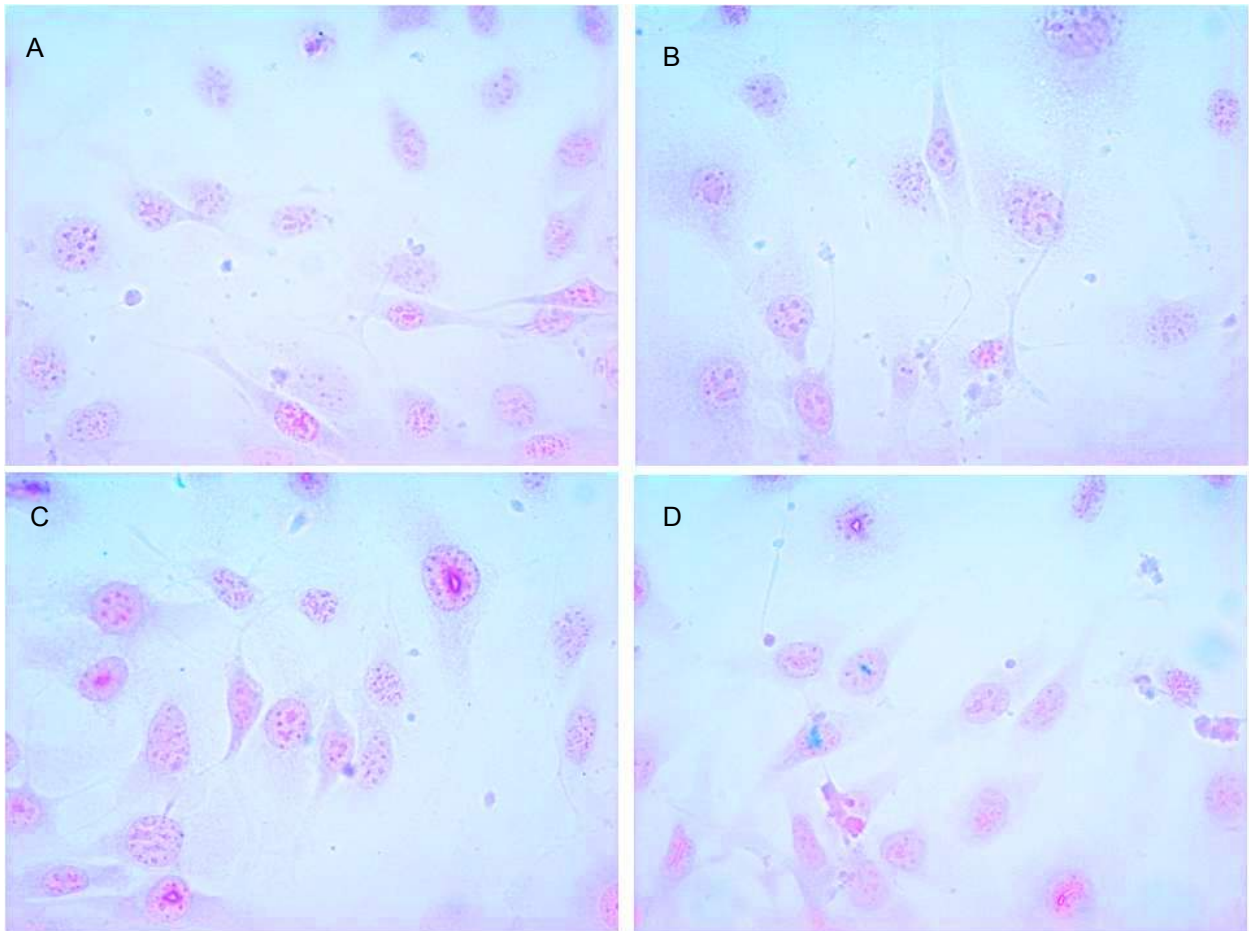


Figure 2: Photomicrographs obtained by light microscopy of bEnd.3 cells labeled with CLIO. Cells were incubated with A) 0.027; B) 0.054; C) 0.1088; D) 0.2175 mg Fe/ml for 24 hours. There is very little blue pigment for all the CLIO concentrations.

3.2 Measurement of iron uptake

In addition to the qualitative test, quantification of cellular iron uptake was done by calorimetric measurement of cell associated iron. The measurements reveal that with increasing particle concentration in the culture supernatant, the cell associated iron concentration increases for every measured time point (Figure 6). For one given concentration, cell-associated iron concentration increases in a time-dependent manner, as was observed with histochemistry (Figures 3, 4, 5).

Experiments were conducted to compare the uptake of the citrate-coated and carboxydextran-coated superparamagnetic particles. The results obtained from murine endothelial cells showed that internalization of citrate particles (VSOP) was approximately 5-10 times higher than that of carboxydextran particles (CMD) when the Fe concentration was varied from 108.8 to 217.5 $\mu\text{g Fe/ml}$ ($P < 0.01$). Maximal internalization of $47.38 \pm 9.76 \mu\text{g Fe}/10^5$ cells occurred with citrate-coated particles (VSOP) at the highest particle concentration of 217.5 $\mu\text{g Fe/ml}$ and an incubation period of 8 hours, while only $6.30 \pm 0.52 \mu\text{g Fe}/10^5$ cells were measured for incubation with carboxydextran-coated particles (CMD). For the other time points, intracellular iron content was also always higher for VSOP than for CMD (46.71 ± 5.05 versus $11.43 \pm 2.23 \mu\text{g Fe}/10^5$ cells 24h incubation, 29.57 ± 0.77 versus $5.25 \pm 1.13 \mu\text{g}/10^5$ cells 2h incubation) (Figures 3A).

At 108.8 $\mu\text{g Fe/ml}$, concentration of internalized iron was 28.5 ± 1.27 versus $6.78 \pm 1.98 \mu\text{g Fe}/10^5$ cells (24h incubation), 21.4 ± 3.93 versus $2.31 \pm 1.23 \mu\text{g Fe}/10^5$ cells (8h incubation) for VSOP and CMD, respectively (Figure 3B). However, at particle concentrations of 27 and 54 $\mu\text{g Fe/ml}$, there was no statistically significant difference ($P > 0.2$) (Figure 3C and D).

A similar set of experiments was performed with HUVEC and THP-1/macrophages. Figure 4 shows that the total uptake of VSOP-C184 increased in a time-dependent

manner by HUVECs. Maximal cellular iron concentration for VSOP was $55.17 \pm 1.46 \mu\text{g Fe}/10^5 \text{ cells}$ at the 24h time point (Figure 4A), which was comparable to the results obtained with bEnd.3 cells, but approximately 30 times higher than that for CMD particles. In contrast, the uptake of VSOP-C184 was lower for the initial 8h, and then increased in the period between 8 and 24h. A trend toward greater uptake of citrate-coated particles was observed at the lower particle concentrations, but P values (0.3) showed no significance (Figure 4B, C and D). In THP-1/macrophages, intracellular uptake of VSOP-C184 also differed significantly from the uptake of CMD at all Fe concentrations (Figure 5). Uptake of nanoparticles increased gradually with the incubation time, except that uptake of CMD at $217.5 \mu\text{g Fe/ml}$ concentration reached a plateau after 8h. As shown in Fig. 5A, citrate nanoparticle VSOP achieved the highest uptake ($22.72 \pm 3.38 \mu\text{g Fe}/10^5 \text{ cells}$) at 24h with highest concentration.

We next evaluated the uptake of CLIO. Murine bEnd.3 cells were incubated with 0.17mg Fe/ml concentration for 2h, 6h, and 24h. The uptake increased slightly from $0.0048 \pm 0.0028 \mu\text{g Fe}/10^5 \text{ cells}$ (2 hours) to $0.0068 \pm 0.003 \mu\text{g Fe}/10^5 \text{ cells}$ (24 hours). These data indicate that there was no significant internalization of CLIO by endothelial cells.

The uptake of nanoparticles was highest for VSOP-C184; then came CMD at $P < 0.01$, which was greater than for CLIO ($P < 0.05$).

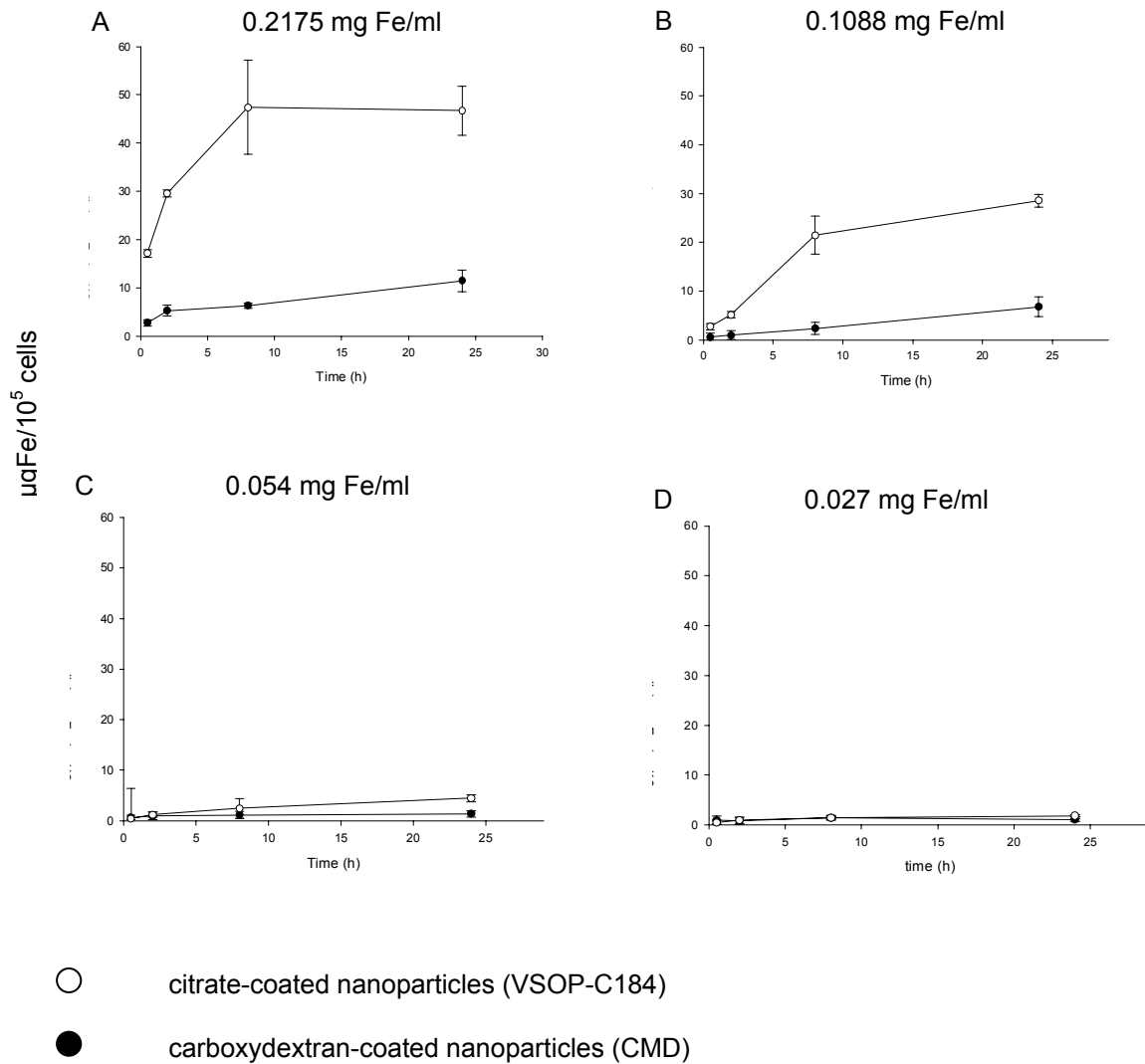


Figure 3: Comparison of uptake of VSOP-C184 and CMD by bEnd.3 cells. Murine endothelial cells (bEnd.3) were incubated with carboxy dextran coated nanoparticles (CMD) or citrate-coated nanoparticles (VSOP-C184). Uptake was measured in the presence of varying concentrations of nanoparticles added to the incubation medium ranging from 0.2175mg Fe/ml (A), 0.1088 (B), 0.054 (C), down to 0.027mg Fe/ml (D).

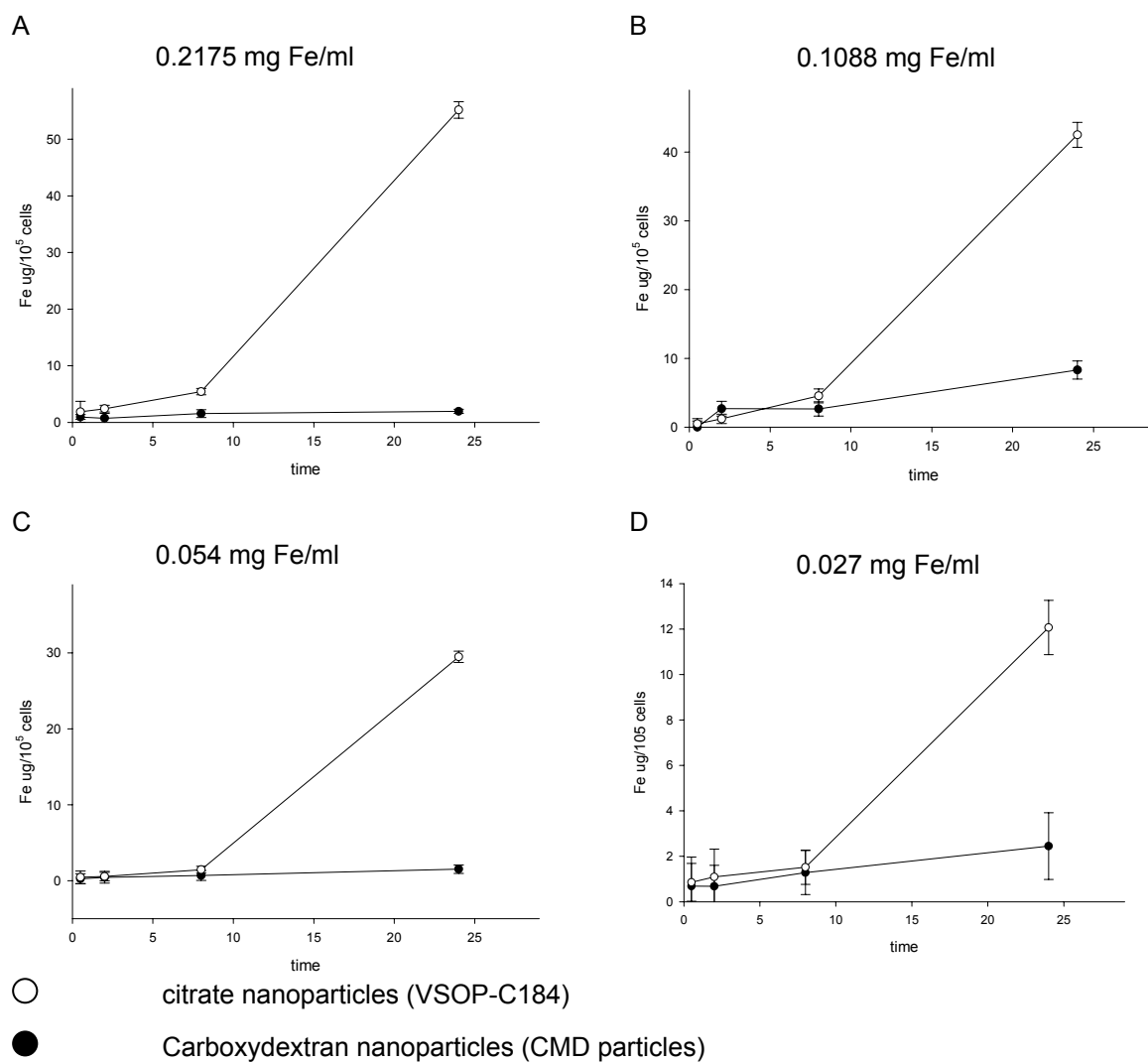


Figure 4: Incubation of HUVEC with carboxydextran nanoparticles (CMD) or citrate nanoparticles (VSOP-C184) 0.2175 mg Fe/ml (A) and 0.1088 (B), 0.054 (C), 0.027 mg Fe/ml (D). Maximal value for VSOP was $55.17 \pm 1.46 \mu\text{g Fe}/10^5$ cells at the 24h point (A), approximately 30 times greater than that of CMD particles.

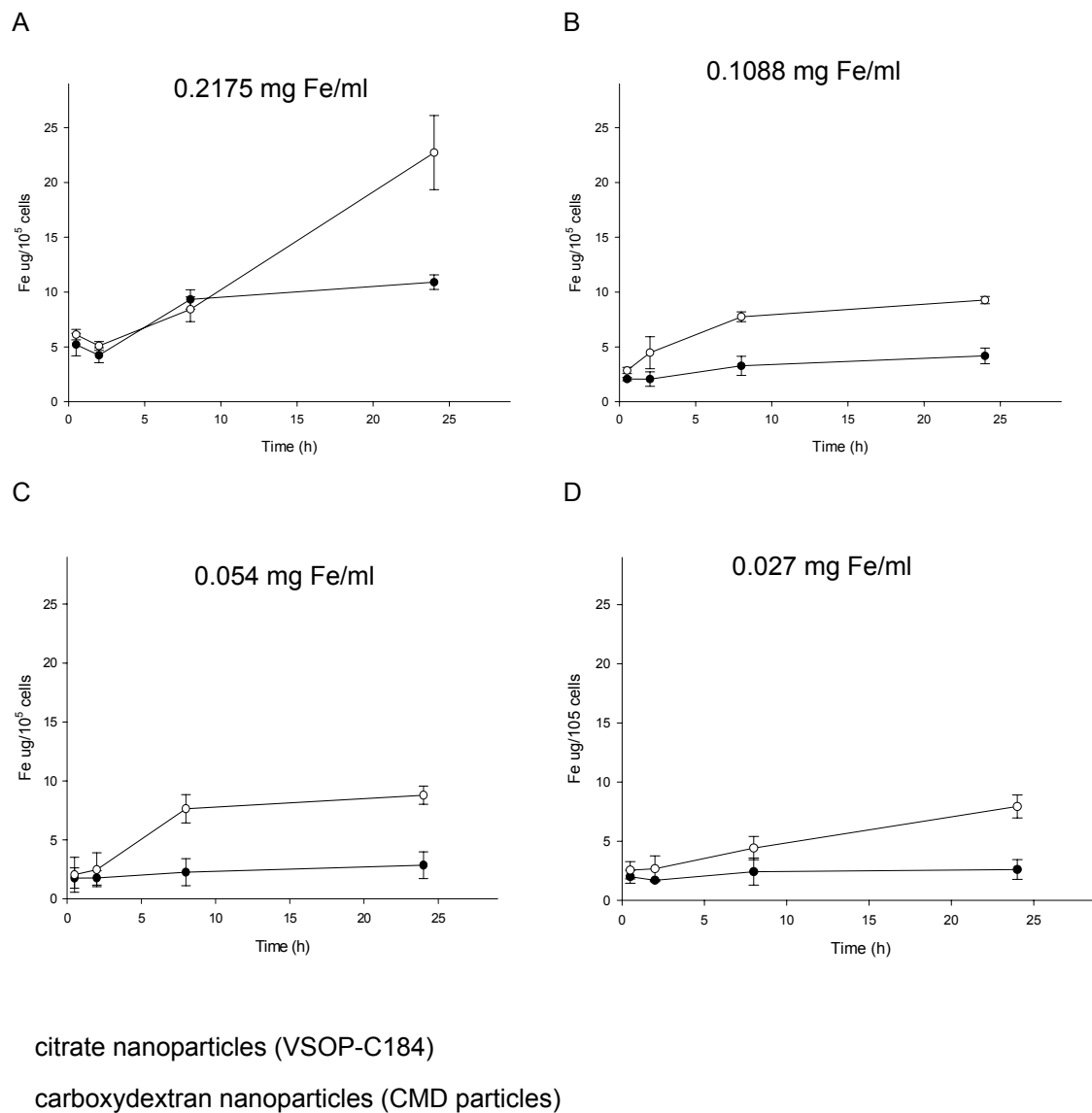


Figure 5: Intracellular iron content of THP-1/macrophages with nanoparticle concentrations (A) 217.5, (B) 108.8, (C) 54 and (D) 27 μ g Fe/ml. Uptake of nanoparticles increased gradually with the incubation time at a higher concentration (A) VSOP-C184 achieved highest values at time point 24h, but CMD reached a plateau after 8h. Data are given as means of 3 measurements \pm SD.

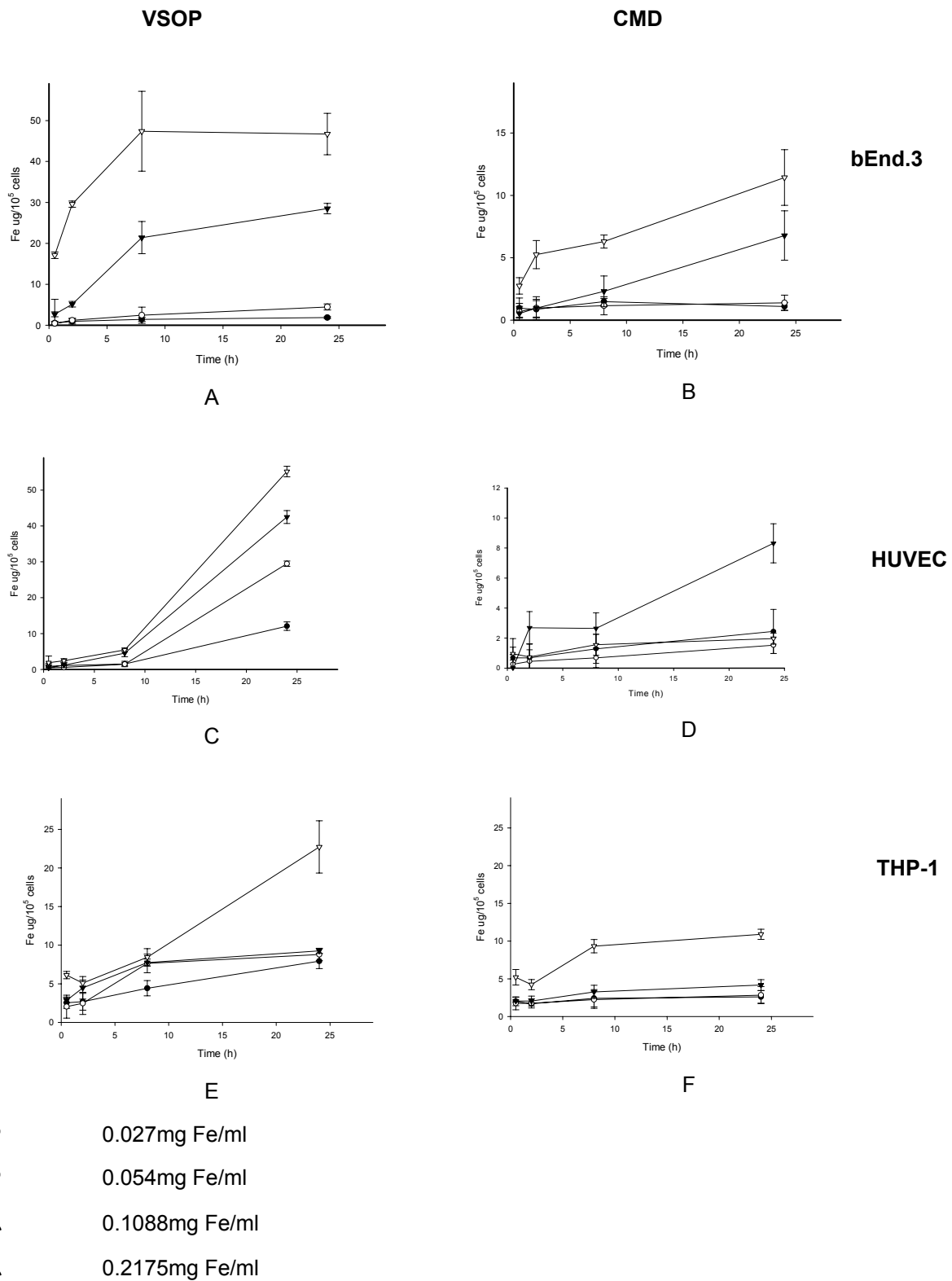


Figure 6: To obtain the concentration and time dependence of the uptake of VSOP (A, C, E) and CMD (B, D, F) by bEnd.3 cells, HUVECs and THP-1/macrophages, the time course of cell labeling is summarized here. Enhanced uptake in mouse endothelial cells is commonly observed because of the higher proliferating activity.

3.2.1 Effect of endocytosis inhibitors

To evaluate the effect of the inhibitors colchicine and cytochalasin B on the VSOP and CMD uptake, the nanoparticles were incubated with endothelial cell monolayers of HUVECs and murine bEnd.3.

After addition of colchicine in both endothelial cells, the uptake of carboxymethyldextran-coated particles CMD was reduced by 50%, whereas the effect of cytochalasin B was only small for CMD (Table 4).

Table 4: Uptake of 24h incubation with CMD. (*) = p<0.05 vs control; (**) = p<0.01 vs control.

EC	CMD particle concentration (mg Fe/ml)	control (µg Fe/10 ⁵ cells)	colchicine (µg Fe/10 ⁵ cells)	cytochalasin B (µg Fe/10 ⁵ cells)
bEnd.3	0.1088	10.6 ± 3.5	6.0 ± 1.1	7.0 ± 3.4
	0.2175	16.1 ± 1.4	6.8 ± 0.7 **	10.6 ± 0.9 **
HUVEC	0.1088	1.3 ± 0.3	0.7 ± 0.2 *	1.2 ± 0.4
	0.2175	3.2 ± 0.6	1.7 ± 0.2 **	3.8 ± 0.5

Table 5: Uptake of VSOP on HUVECs. (*) = p<0.05 vs control; (**) = p<0.01 vs control.

H U V E C	Incubation time	VSOP particle concentration (mg Fe/ml)	control (µg Fe/10 ⁵ cells)	colchicine (µg Fe/10 ⁵ cells)	cytochalasin B (µg Fe/10 ⁵ cells)
	24h	0.1088	14.8 ± 1.9	17.0 ± 4.0	8.8 ± 1.0 **
		0.2175	43.1 ± 10.3	15.3 ± 1.5 **	24.0 ± 1.9 *
	2h	0.1088	2.1 ± 0.3	2.7 ± 0.3	1.3 ± 0.2 **
0.2175		15.8 ± 1.3	12.6 ± 5.7	5.5 ± 2.8 **	

The reverse was true for the intracellular uptake of VSOP. The VSOP-C184 uptake in HUVEC treated with cytochalasin B was significantly inhibited (40%-65%) compared with that of the control group (P<0.01). But colchicine did not induce any major changes (Table 5).

No effect of either colchicine or cytochalasin B was observed for the uptake of citrate-coated particles VSOP on bEnd.3 cells (Figure 7).

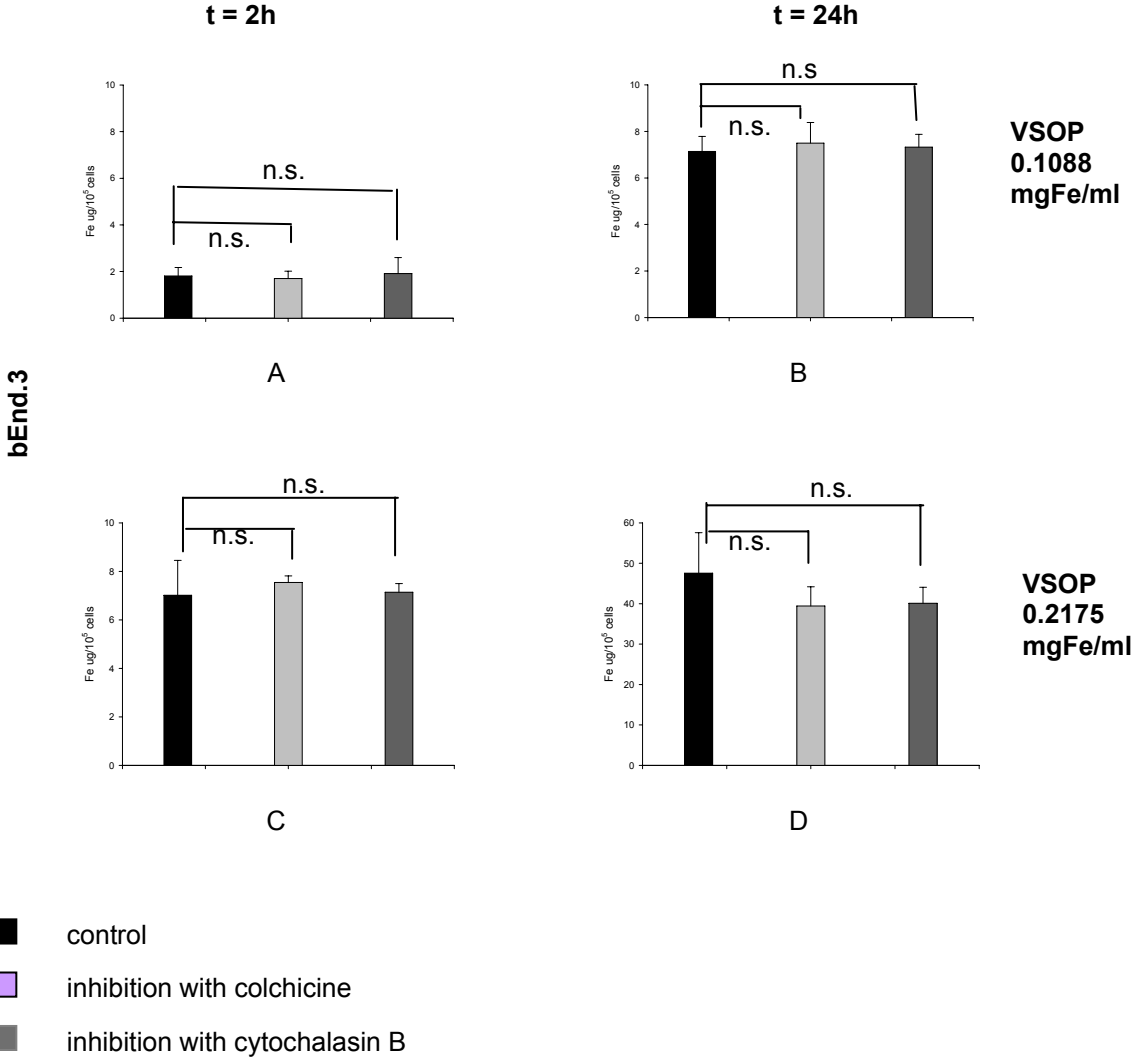


Figure 7: Uptake of VSOP on murine bEnd.3 cells (in $\mu\text{g iron}/10^5$ cells) after different pre-treatment of the cells and subsequent incubation for 2h (left-hand panel) and 24h (right-hand panel) at 0.1088mg Fe/ml (A, B) and 0.2175mg Fe/ml (C,D) VSOP concentration. Before addition of VSOP, the cells were incubated with the cytoskeleton inhibitor colchicine or with cytochalasin B. No significant difference was observed between the uptakes in these groups. "Control" = bEnd.3 cells incubated without addition of inhibition. "Inhibition with colchicine or cytochalasin B" = bEnd.3 cells pretreated with 50 $\mu\text{g}/\text{ml}$ colchicine or 5 $\mu\text{g}/\text{ml}$ cytochalasin B for 4 hours. Error bars represent the standard deviation of the mean for a sample size of $n = 3$. n.s. = not significant.

3.3 Flow cytometry measurement

Flow cytometry was used to characterize the specific binding of CLIO monoclonal antibody (mAb) complexes.

First, we tested unstimulated murine endothelial cells (bEnd.3) with anti-CD62E-PE to measure CD62E expression on unstimulated cells. Histograms were derived from gated events (R1) (Fig. 8A) with the forward and side light-scatter characteristics of viable murine endothelial cells. We used rIgG2 α -PE in the same experiment at the same dose as immunoglobulin isotype controls (Fig. 8B). CD62E were expressed at relatively lower levels by the unstimulated cells.

bEnd.3 cells were stimulated with mouse TNF- α (500U/ml) for 4 hours. This stimulation time is based upon several previous studies, which demonstrate that endothelial cells treated with TNF- α express peak levels of CD62E at 4 hours (²¹). After 4 hours mTNF- α stimulation, murine endothelial cells were labeled with anti-CD62E-PE versus rIgG2 α -PE. CD62E expression of stimulated cells was 5.2-fold (median) and 3.8-fold (geometric mean) higher than that of unstimulated cells (Fig. 8C).

FACS analysis demonstrated a significant shift in fluorescence for the stimulated cells labeled with CLIO-antiCD62E. CLIO-antiCD62E (nanoparticles-antiCD62E + second-mAb-FITC) bound with specificity to mTNF- α stimulated murine endothelial cells. When we labeled CLIO-antiCD62E with unstimulated and stimulated murine endothelial cells for 30 minutes; fluorescence median of unstimulated cells was 6.7 and fluorescence mean 5.5 (Fig. 8D). Fluorescence median and mean of stimulated cells were 26 and 25, respectively (Fig. 8E). CLIO-antiCD62E binds specifically to stimulated bEnd.3 cells displaying a 3.9-fold (median) and a 4.5-fold (mean) increase of fluorescence compared to unstimulated cells.

Table 6: Binding of CD62E and CLIO antiCD62E to murine endothelial cells (bEnd.3)

antibody (-conjugate)	mock treatment		TNF α -stimulation		TNF / mock X fold increase (median/ mean)
	Netto median	Netto Gmean	Netto median	Netto Gmean	
rat anti- mouseCD62E / rat IgG2a-PE	57	77	296	295	5.2 / 3.8
CLIO- antiCD62E/ CLIO-rat IgG2a	6.7	5.5	26	25	3.9 / 4.5

Incubation time was quite short (30 minutes) and temperature during incubation was kept low (5°C) in order to reduce unspecific uptake of CLIO-antiCD62 by endothelial cells.

bEnd.3 cells express no CD40; therefore we used mouse splenocytes to test CLIO-anti-CD40. Fig.9A shows dot plots of mouse splenocytes. The gate was set to include cells that had the forward and side light-scatter characteristics of B-lymphocytes. Mouse splenocytes were labeled with the anti-mouse-CD40-PE versus isotype control rIgG2a-PE (Fig.9B and C). 42.3% of mouse splenocytes bound to antiCD40-PE, whereas only 0.8% of the cells bound to non-specific rIgG2a-PE.

Incubation with CLIO-antiCD40 showed results comparable to those with CLIO CD62E conjugate (Fig. 9D and E). Mouse splenocytes were labeled with CLIO anti-mCD40 or CLIO-rIgG2a (+ second-mAb-FITC); and fluorescence intensity was 2-fold higher than that of CLIO-rIgG2a-incubated cells. CLIO antiCD40 specifically bound to

32.3% mouse splenocytes while antiCD40-PE (without nanoparticles) bound to 42.3% splenocytes.

Table 7: Binding of CD40 and CLIO-antiCD40 to mouse spleen cells

Treatment	M1 of R2	Median (M1)	Gmean (M1)	Median (R2)	Gmean (R2)
rlgG2a	0.8%	461	856	18.6	16.3
AntiCD40	42.3%	1779	1734	69.8	172.4
CLIO-rlgG2a	6.5%	299.6	362.5	11.5	15.9
CLIO-antiCD40	32.5%	368.5	409.4	17.3	36.9

As expected, the binding of CLIO-antibody conjugate to mouse cells is specific; non-specific binding of CLIO-rlgG2a is significantly lower. Thus, we demonstrated that the binding affinity of CLIO-antibody conjugate and anti-mCD62E/ anti-mCD40-PE (without nanoparticles) to mouse cells is comparable. This suggests that the binding affinities of CD62E and CD40 are not significantly reduced after conjugation to CLIOs.

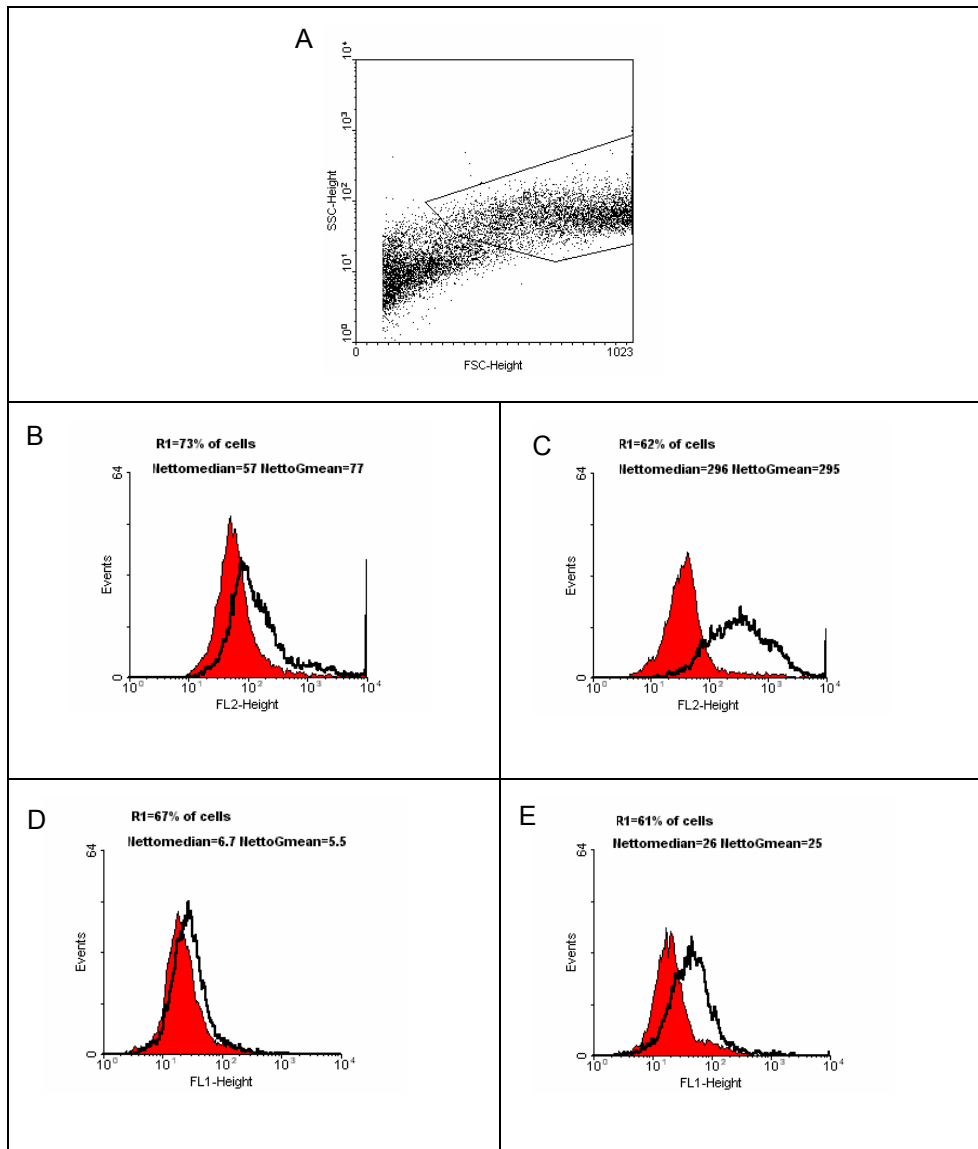


Figure 8: Dot plot of murine endothelial cell line (bEnd.3) (A). The intensity of side light-scatter (y-axis) was plotted against the intensity of forward light-scatter (x-axis). The gate was set to eliminate cell debris. (B) Unstimulated bEnd.3 cells were labeled with anti-CD62E-PE versus rlgG2a-PE. The data were shown as white histograms of the PE-channel for cells labeled with anti-CD62E, while isotype control (rlgG2a) was displayed by the red shaded peak. (C) FACS histograms of stimulated bEnd.3 cells. After 4 hours of mouse-TNF α stimulation, murine endothelial cells were labeled with anti-CD62E-PE (white) versus rlgG2a-PE (red). CD62E is expressed at higher levels on stimulated cells. Median increased from 57 to 296 AU (increase 5.2 fold) with the PE-labeled antibody. Unstimulated (C) and stimulated (D) bEnd.3 cells were labeled with CLIO-antiCD62E versus CLIO-rlgG2a [+goatF(ab')₂-anti-rat IgG(H+L)-FITC]. Whereas there was a clear shift in the mean fluorescence intensity of stimulated cells stained with CLIO-antiCD62E, fluorescence increased from 6.7 to 25 3.8-fold increase. Thus, CLIO-antiCD62E are specifically bound to stimulated bEnd.3. PE = phycoerythrin FITC = fluorescein isothiocyanate.

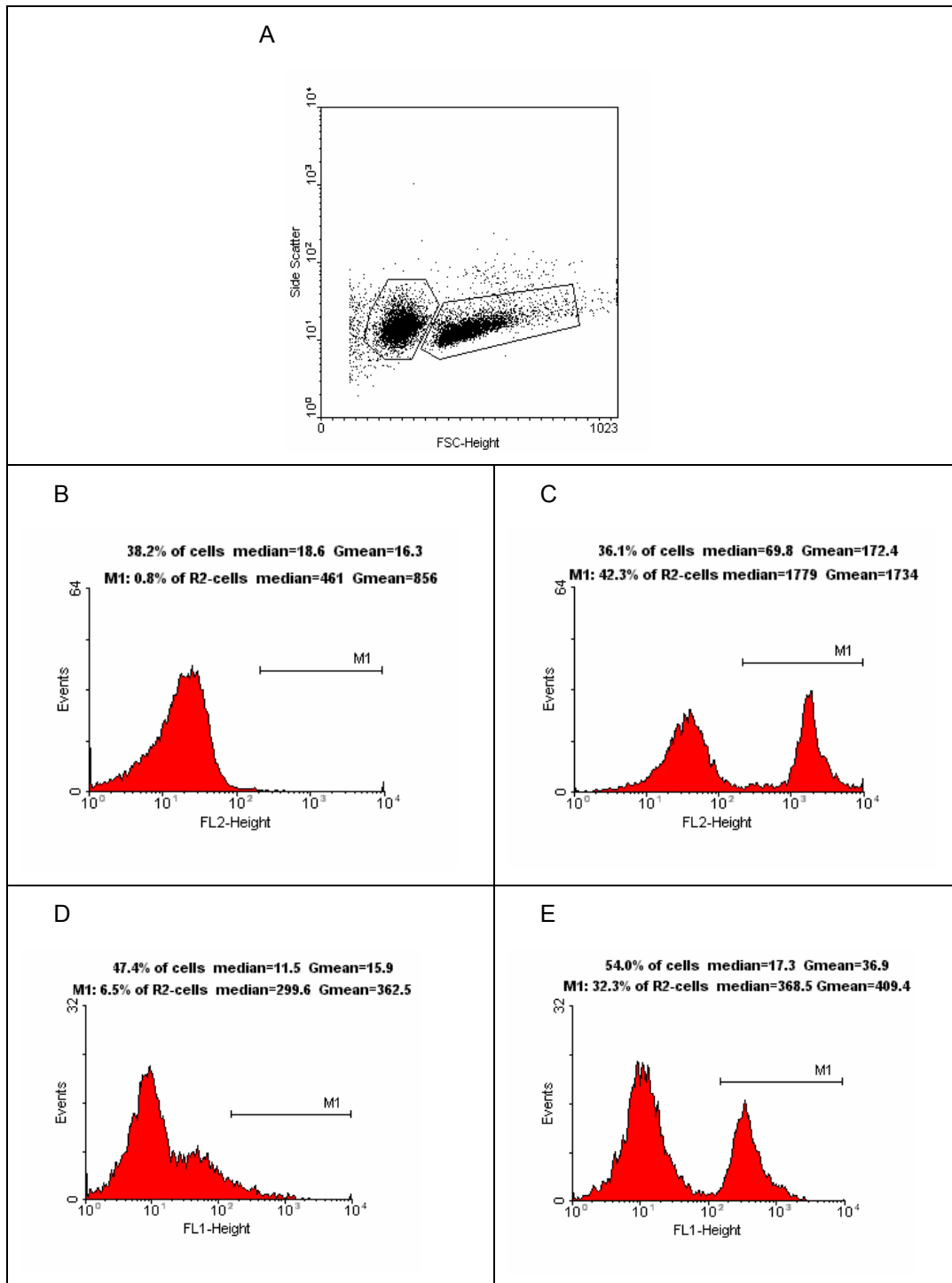


Figure 9: Dot plots and histogram plots of mouse splenocytes. The gate (R2) was set by the forward and side light-scatter characteristics of B-lymphocytes (A). Mouse splenocytes were labeled with the anti-mouse-CD40-PE (C) versus isotype control rlgG2a-PE (B). With the chosen gate settings only 0.8% of the cells were within the gate after staining with non-specific rlgG2a-PE, while 42.3% mouse splenocytes were within the gate with CD40-PE. A similar set of experiments was performed with CLIO-anti-mCD40. Mouse splenocytes were labeled with CLIO anti-mCD40 (E) or CLIO-rlgG2a (D). Fluorescence intensity increased compared to that of CLIO-rlgG2a-incubated cells. Median fluorescence increased from 300 AU to 368 AU.

4 Discussion

Uptake of citrate- and dextran-coated superparamagnetic iron oxide particles by endothelial cells and macrophages revealed that unspecific uptake is dependent on the cell surface coating of the nanoparticles.

Use of nanoparticles linked to the monoclonal antibodies anti-CD40 and anti-CD62E demonstrated that these antibody-SPIO complexes bind more strongly specifically to certain cell surface proteins compared to isotype IgG antibodies.

4.1 Discussion of methods

4.1.1 Why was CD40 and CD62E monoclonal antibody chosen for specific labeling?

During the last decade, atherosclerosis was been increasingly understood as a chronic degenerative inflammatory disease. Key elements of chronic inflammation such as the presence of cytokines and leukocytes, mainly monocytes, and increased expression of adhesion molecules, are observed in atherosclerotic plaques. Conventional risk factors such as hypercholesterolemia, hypertension or cigarette smoking are thought to trigger, and at the same time modulate, the disease.

CD40 is a cell surface protein belonging to the TNF receptor family. It is expressed constitutively on B-lymphocytes. The corresponding ligand (CD40L or CD154) has been cloned and identified as a CD4⁺ T-cell activation antigen. CD40 – CD154 interactions play a critical role in the regulation of both humoral and cellular immunity. However, CD 40 is also expressed on cells outside of the immune system, such as endothelial cells, fibroblasts, and smooth muscle cells. Several studies have

established a link between CD40-CD154 interactions and inflammatory reactions in disease. Similarly, the importance of CD40-CD154 interactions in the development of atherosclerosis has been demonstrated in animal studies, but also in humans from data derived from clinical studies.

Mach and colleagues ⁽²²⁾ fed LDL-receptor knockout mice a high-cholesterol diet and used a CD154 antibody to block CD40 and CD154 signalling. They observed that this antibody reduces the size of aortic atherosclerotic lesions by 59% and their lipid content by 79%. Furthermore, atheromas of mice treated with anti-CD40L antibody contained significantly fewer macrophages (64%) and T lymphocytes (70%), and exhibited decreased expression of vascular cell adhesion molecule-1. Similar effects were reported by Lutgens et al. ⁽²³⁾, who used Apo-E knockout mice. They inhibited CD40-CD154 signaling by an anti-CD154 antibody also and found that T-lymphocyte content was significantly decreased in atherosclerotic lesions. Furthermore, a pronounced increase in collagen content, vascular smooth muscle cell / myofibroblast content and fibrous cap thickness was observed.

In human atherosclerotic plaques, CD40 and CD154 were found to be expressed whereas in normal vascular tissues they were not ⁽²⁴⁾, and the expression of CD40 correlated with the severity of the plaques ⁽²⁵⁾. Clinical studies showed that patients with acute coronary syndromes exhibit enhanced blood levels of soluble and membrane-bound CD40L ⁽²⁶⁾. Moreover, high levels of soluble CD40L were associated with increased cardiovascular events in women, suggesting that CD40 activation may be involved in the development of acute coronary syndromes ⁽²⁷⁾.

E-selectin is one of the adhesion molecules participating in mediating interactions between leukocytes and endothelial cells ⁽²⁸⁾. It is induced by cytokines such as TNF- α or interleukin (IL)-1 and by lipopolysaccharide (LPS) ^(29;30). Maximal levels of E-selectin protein are expressed at the cell surface, after it has been induced and stimulated for 3-4 hours ⁽³¹⁾. Apart from its role in acute inflammation for the recruitment of neutrophils, E-selectin has been found to be expressed in

atherosclerotic plaques also (³²). The severity of E-selectin expression was shown to correlate with the severity of the atherosclerotic lesion (^{32,33}).

Wagner and colleagues used LDL receptor negative mice and evaluated the role of E- and P-selectin for atherosclerosis in these mice by generation of mice that lacked E- and P-selectin on the background of LDLR negative mice (³⁴). After 22 weeks on a high cholesterol diet, the mice had lesions throughout the aorta but this process was delayed in LDLR^{-/-} P/E^{-/-} mice. At 37 weeks on the diet, the lesions progressed to the fibrous plaque stage in both genotypes. However, the lesions in the aortic sinus in LDLR^{-/-} P/E^{-/-} mice were 40% smaller and less calcified than those of LDLR^{-/-} P/E^{+/+} mice. These data suggest that P- and E-selectin together play an important role in both early and advanced stages of atherosclerotic lesion development.

Thus, the expression of both cell surface molecules can be linked to the severity of atherosclerotic lesions and may serve as a target for molecular imaging of atherosclerotic lesions.

4.1.2 Why were human umbilical vein endothelial cells, the mouse endothelial cell line bEnd.3 and human macrophages chosen for measurement of unspecific uptake of nanoparticles?

We examined the uptake of nanoparticles with different surface chemistry by human umbilical vein endothelial cells (HUVEC), the mouse endothelial cell line bEnd.3, and a human macrophage cell line (THP-1 cell).

Human umbilical vein endothelial cells (HUVEC) and bEnd.3 are both endothelial cells. Monolayers of cultured HUVEC have been used for decades in in vitro models to investigate endothelial function. Endothelial cells line the inner surface of all vessels and thus form an interface between blood and tissues. Apart from serving as

an anticoagulant surface⁽³⁵⁾, they participate in the regulation of vascular tone by secretion of several vasoactive substances⁽³⁶⁾ and, in addition, they participate in the recruitment of leukocytes into surrounding tissue⁽³⁷⁾. HUVECs are of embryonic origin and may therefore not be an optimal model for investigation of diseases occurring in adults (e.g. atherosclerosis); however, they are widely used and well characterized.

The mouse endothelial cell line bEnd.3 is of mouse origin and immortalized by the middle-T oncogene⁽³⁸⁾. It was chosen as an in vitro model for mouse endothelium since this cell line can express E-selectin upon activation by TNF- α ⁽³⁹⁾ and has been also used for other in-vitro investigations, e.g., the investigation of the blood-brain barrier⁽⁴⁰⁾.

The human monocytic cell line THP-1 can be differentiated by 100 nM PMA treatment (48 hours) to THP-1 macrophages⁽⁴¹⁾ and thus may serve as a model of macrophages in vitro.

4.1.3 Rationale for the iron concentrations of nanoparticles used

To compare cellular uptake in HUVEC, bEnd.3 and THP-1 cell lines, we used each nanoparticle at concentrations of 0.027 up to 0.218 mg Fe/ml. These concentrations were chosen according to MRI measurements made previously at our institution. From serial dilutions of iron nanoparticles, a range of concentrations was chosen to cover the detection limit of the particles by MRI. These concentrations of iron were non-toxic for the three cell types in culture for up to 24 hours as judged from cell morphology. Cell death through apoptosis may start with only minor changes in cell morphology but was not investigated in this setting^(42;43). Cells appeared unchanged in morphology and were still attached to the culture plate after the incubation period, which suggests that the cells were still living.

4.2 Characterization of iron oxide particles

4.2.1 Unspecific uptake

Superparamagnetic iron oxide particles of different size and composition have been developed and used as contrast media for magnetic resonance (MR) imaging for approximately 15 years⁽⁴⁴⁾. Agents with a large particle diameter of 50 nm are suitable for imaging tumors of the liver and spleen⁽⁴⁵⁾, whereas so-called ultra small (USPIO) particles with a diameter of approximately 20 nm are being tested as contrast media for MR lymphography⁽⁴⁶⁾ and MR angiography⁽⁴⁷⁾. Other potential areas for applying iron oxide particles include the characterization of vulnerable plaques⁽⁴⁸⁾ and, similar to conventional iron oxide particles, also liver imaging⁽⁴⁹⁾. The particles have to be coated with an organic layer that prevents their aggregation and determines their pharmacokinetic properties and tolerability. In addition, the size and surface structure determines the T1- and T2-shortening effects of the particles⁽³⁾. All SPIO particles that have so far undergone preclinical or clinical testing are coated with an organic polymer, such as dextran⁽⁴⁷⁾, carboxydextran⁽⁵⁰⁾ or polyethylene glycol⁽⁵¹⁾ or with citrate⁽⁵²⁾. Polymer coating may impair the tolerability of the particles, which has in particular been shown for dextran^(53;54) and limits the minimal overall particle size that can be achieved. Nanoparticle uptake by cells is regulated by a number of factors. The size, charge, and surface chemistry of nanoparticles strongly influence their biodistribution⁽⁵⁵⁾.

Labeling of cells has been used to track cells in vivo, e.g., for the tracking of rat T-cells⁽⁵⁶⁾. These labeled cells can be detected in vivo by MR imaging⁽⁵⁷⁾. Uptake of dextran-coated iron particles is limited by the fact that many cells, such as lymphocytes, do not possess high-efficiency internalizing receptors⁽⁵⁸⁾. Therefore, several approaches to increase cellular uptake have been evaluated. Josephson et al. linked a peptide from the HIV genome to the particles, which greatly enhanced the uptake of iron oxide particles⁽⁵⁹⁾. Fleige et al. demonstrated that particles coated with citrate are more efficiently internalized by macrophages than carboxydextran-

coated particles.

By contrast, for the labeling of cell surface proteins by coupling of peptides or antibodies to the iron oxide particles, low internalization is desirable to prevent unspecific labeling of cells (^{60;61}).

In the present study, two different dextran-coated particles and one citrate-coated preparation were compared concerning their biological and magnetic properties. The endothelial cells from humans and mice as well as human macrophages were incubated for different periods and different time intervals with the different particle suspensions. The cellular uptake was semi-quantitatively measured using Prussian blue staining and in addition quantitatively by cellular iron content. Both methods suggested that citrate-coated particles are much more extensively and more rapidly internalized than dextran-coated particles.

These data are in agreement with those of the above cited publication by Fleige et al. (⁶²) in which they reports that intracellular iron concentrations were about 10-fold higher with citrate-coated particles compared to carboxydextran-coated particles. Davda et al. used a DL-lactide-co-glycolide polymer coated particle preparation and demonstrated by confocal microscopy that internalized particles were localized mostly in the cytoplasm and not simply bound to the cell surface (⁶³). Therefore, we hypothesize that citrate-coated particles and carboxydextran-coated particles are internalized into the cytoplasm also.

Our experiments were done with a much longer incubation time than in previously published studies. In our experiments, after 2 hours incubation only a small difference in iron uptake between citrate-coated and dextran-coated particles was apparent. However, with increasing time, uptake of dextran-coated particles increased only slightly and reached a plateau-like phase. Citrate coated particles were internalized more rapidly and did not reach a plateau. Cellular iron concentrations of citrate-

coated particles were 5-30 times higher than those of dextran-coated particles. The results obtained from Prussian blue staining point in the same direction. Citrate-coated particles were internalized much faster and to a higher degree than dextran-coated particles. This was true for all tested cell types, human and mouse endothelial cells and macrophages.

Fluid-phase endocytosis is more prominent in proliferating cells than in resting cells. bEnd.3 mouse endothelial cells proliferate faster than HUVEC. Interestingly, uptake of iron particles by bEnd.3 was significantly higher than by HUVEC.

4.2.2 Uptake inhibited by colchicine and cytochalasin B

Further evidence of a role for endocytosis in unspecific uptake was obtained with the use of colchicine and cytochalasin B.

Colchicine and cytochalasin B alter microtubule and microfilament structure and function. The microtubules are required for fluid-phase endocytosis and microfilaments hinder this process (⁶⁴).

Colchicine disrupts cellular microtubules. In confluent endothelial monolayers, colchicine induces a change of microfilament distribution with a loss of dense peripheral bands, an increase in actin microfilament bundles, and an associated increase in focal adhesion proteins at the periphery of the cells. However, when microfilaments were disrupted with cytochalasin B, microtubule distribution remained unaltered (⁶⁵). Colchicine suppresses unspecific pinocytosis, while cytochalasin B inhibits phagocytosis (^{66;67}).

Due to the size of the particles, their tendency to aggregate and the stability of the dextran coat (cross linking), dextran coated particles in general are incorporated into cells by three mechanisms: phagocytosis, fluid-phase (pinocytosis) and the receptor-mediated endocytotic pathway (^{68,69}). Pinocytosis involves membrane ruffles that extend and enclose extracellular fluids, bringing its contents into the cell (⁷⁰). Phagocytosis is the process of internalization of particles by cells endowed with phagocytic activity.

The present study provides in vitro evidence that the carboxydextran-coated SPIO uptake by endothelial cells is reduced by colchicine (50%). Conversely, cytochalasin B down-regulates the endocytosis of citrate-coated particle. Our data imply that the major mechanism of uptake would be phagocytosis for the VSOP and pinocytosis for the carboxydextran-coated particle CMD.

Our inhibition data are in agreement with those of a previous report on the uptake of nanoparticles by macrophages. Fleige et al. investigated macrophages treated with cytochalasin B and found that the latter did not reduce the uptake of dextran-coated particles but significantly reduced the incorporation of the citrate-coated particles (by approximately 17%). After incubation with colchicines, the reverse was seen: A significant reduction by approximately 40% for dextran-coated particles compared with control cells, whereas no effect for the citrate-coated particles was observed (⁶⁶).

In contrast, the investigation by Sundstrom (⁷¹) showed that pretreatment with colchicine did not affect the labeling of cells by dextran-coated superparamagnetic iron oxide nanoparticles. Qaddoumi et al. (⁷²) incubated polymer-based nanoparticles with rabbit primary conjunctival epithelial cells and observed that uptake of these particles was inhibited by cytochalasin D while a microtubule inhibitor similar to colchicine had no significant effect. These polymer-based nanoparticles apparently behaved similarly to the Dextran-coated particles.

Interestingly, pretreatment of bEnd.3 cells with either colchicines or cytochalasin B did not significantly reduce the VSOP uptake. Particles were incorporated by murine endothelial cells in the presence of these inhibitors. This probably reflects a combination of different mechanisms: i) bEnd.3 cell line is a murine endothelioma cell transformed by infection with the NTKmT retrovirus vector that expresses polyomavirus middle T-antigen (³⁸); ii) the acquisition of VSOPs by the cells through alternative pathways is not blocked by the particular inhibitor.

A dextran-coated iron oxide (150 nm) and carboxydextran-coated SPIOs of various hydrodynamic diameters (17-65 nm) were recently tested in human cancer cell lines, resulting in a substantial uptake of iron oxides (up to 5 µg Fe per 1×10⁵ cells) (⁷³). Although endocytosis is affected by particle size (^{74;75}), the intracellular uptake of dextran-coated particles (150 nm) did not significantly differ from uptake of carboxydextran-coated particles (65 nm). Therefore, the particle coating will be of major importance for cell-tagging efficacy, which is also confirmed by our data.

In summary, it has been shown by measurement of iron uptake that a modified surface can influence not only the quantity of internalization, but also the pathway of endocytosis. Endocytosis represents one, but not the only, mechanism of nanoparticle uptake by endothelial cells.

4.2.3 Specific binding of antibody-CLIO conjugate

Superparamagnetic iron oxide particles have been used as a contrast agent for MRI for almost a decade (⁹). The popularity of superparamagnetic iron oxide particle labeling is due to the following properties:

(1) These particles provide the greatest change in signal (albeit hypointensity) per unit of metal, in particular on T2*-weighted images. Since they are composed of

thousands of iron atoms, their sensitivity is more favorable than that of the other contrast agents used in MRI;

(2) These particles are composed of biodegradable iron, which is biocompatible and can be absorbed by cells using normal biochemical processes;

(3) The coating surface, usually dextran, allows covalent coupling of functional groups and ligands;

(4) They can be easily detected by light and electron microscopy;

(5) Since they have magnetic properties, they can be magnetically controlled based on their size with potential to reveal their structural (bound) conformation.

In order to prevent aggregation, iron oxide nanoparticles require stabilization. Most commonly this is accomplished by a surface coating with dextran. This coating enhances the blood circulation time and stabilizes the colloidal particle solution (1;11;76).

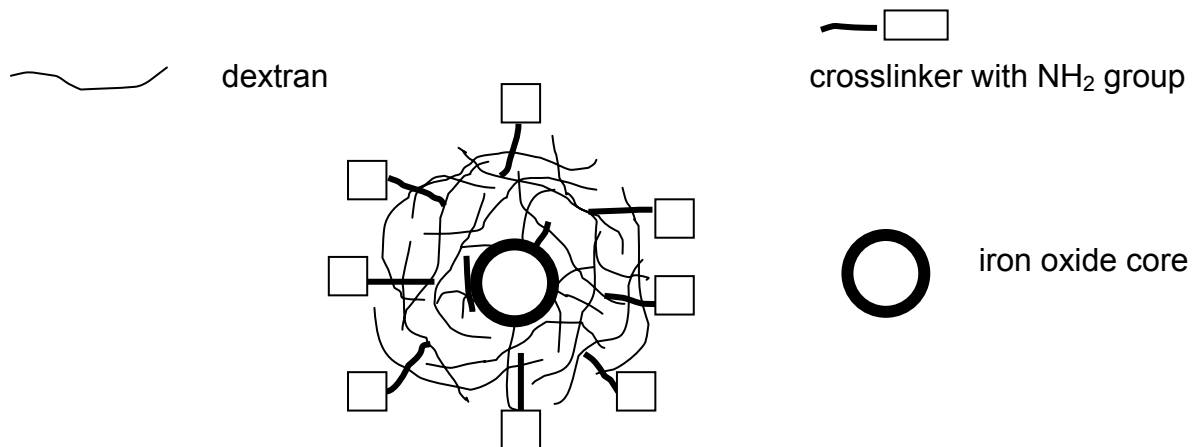


Figure 10: aminated CLIO = dextran coated, Cross-Linked and aminated Iron Oxide particles = CLIO-NH₂

One widely used iron oxide particle for in vivo and in vitro experiments is CLIO (cross-linked iron oxide) (59;77). The core of CLIO is a single iron oxide crystal held within a stable dextran coat that isolates it from surrounding solutions and lowers protein adsorption to the particle surface.

CLIO particles have a relatively long blood half-life (655 ± 37 min in mice at a dose of 10mg Fe/kg) (⁶¹).

Molecular imaging uses iron oxide particles with a modified coat. Receptor-directed imaging and cell labeling for in-vivo monitoring of cell migration (e.g. stem cell labeling, and labeling of gene constructs for localization in genetic therapy) are examples of molecular imaging applications (⁷⁸). Usually, a peptide or an antibody is linked to the CLIO to accomplish specific binding to the target structure (^{18;61}).

Another means of generating nanoparticles for molecular imaging was introduced by Fayad et al. (⁷⁹). A high-density lipoprotein (HDL)-like construct with a small size (9 nm diameter) was generated and coupled to Gd-DTPA-DMPE. This particle is biodegradable, does not trigger immunoreactions and is not recognized by the mononuclear phagocytic system (MPS) / reticuloendothelial system (RES). Further experiments have to prove its suitability for in vivo applications.

Winter et al. formulated paramagnetic nanoparticles targeted at $\alpha_v\beta_3$ -integrins. Each particle (ca. 273 nm in diameter) contained approximately 90 000 paramagnetic chelates (gadolinium-diethylenetriamine pentaacetic acid-bis-olate [Gd-DTPA-BOA]) (⁸⁰). A vascular lesion was induced in New Zealand white rabbits fed with 1% cholesterol for approximately 80 days. Alpha (v) beta3-integrin-targeted nanoparticles were injected intravenously and provided specific detection of the neovasculature within 2 hours by routine magnetic resonance imaging (MRI) at a field strength of 1.5 T. Increased angiogenesis was detected as a 47+/-5% enhancement in MRI signal averaged throughout the abdominal aortic wall among rabbits that received alpha(v)beta3-targeted paramagnetic nanoparticles.

These data prove that in vivo imaging with specific contrast agents is feasible.

For the current experiments an approach as described previously was chosen: CD40 and CD62E antibodies were linked to CLIO particles and tested in vitro. This was

done with murine endothelial cells activated by TNF- α to test binding to CD62E and with murine splenocytes which constitutively express CD40 to test binding to CD40. Binding of the CLIO-antibody construct was detected by incubation with secondary fluorescence labeled antibodies directed against the CLIO-linked CD40 or CD62E antibody, respectively, and analyzed by flow cytometry (FACS).

Since these experiments were planned in conjunction with in-vivo experiments in mice all binding assays were done with murine cells. The cells were incubated for 30 minutes with the different antibody-nanoparticle preparations to keep unspecific binding low. From our in-vitro experiments which measured iron uptake by endothelial cells it was apparent that only small amounts of dextran-coated particles are internalized by the cells. This observation was confirmed by the FACS measurements where a small background signal was detectable with IgG-linked particles which served as negative controls. In contrast, CLIO linked to CD40 antibodies or to CD62E antibodies bound significantly better than IgG-linked CLIO. This was true especially for the anti-CD40-CLIO constructs where fluorescence increased 2-fold. Comparable results were observed with anti-CD62E-CLIO constructs; however, increase in fluorescence was higher than with CD40 binding; it increased 3.9-fold (median) and 4.5-fold (mean).

Data derived from HUVECs showed that CD62E expression measured by FACS increased about 100-fold upon activation by TNF α . The lower binding of anti-CD62E-CLIO to murine bEND.3 cells might be due to several factors e.g. to a lower affinity of the antibody used or alternatively to lower expression of CD62E following activation by TNF α . The anti-CD62 antibody (clone 10E6) was obtained from Prof Vestweber and had been evaluated extensively (⁸¹). The activation of bEnd.3 cells was described in a previously published study (³⁹). However, only mRNA data by Northern blotting or competitive PCR are presented in this paper. Therefore, a real comparison is not feasible.

TNF- α is a pleiotropic proinflammatory cytokine produced mainly by activated

macrophages (^{82;83}). In 1975, it was first reported as mimicking the tumor necrosis of endotoxin itself, and was named tumor necrosis factor.

The expression of E-selectin and CD40 on the murine endothelial cell line bEnd.3 was reported before, but to our knowledge only on the mRNA level (³⁹). Therefore, E-selectin expression was again evaluated by FACS analysis. bEnd.3 cells were stimulated with mTNF. E-selectin expression was highest at 4 hours, as has been reported previously for human endothelial cells in culture (²¹). mTNF α stimulated bEnd.3 cells were used to evaluate binding of CLIO-CD62E versus CLIO IgG2a, showing similar binding to CD62E antibodies alone.

CD40 was not expressed by resting bEnd.3 cells either by stimulation with mTNF α or by stimulation with murine interferon- γ . Therefore, mouse splenocytes were used to evaluate CLIO-CD40 binding. CLIO labeled with anti-mCD40 antibodies was tested versus CLIO-rIgG2a (+ second-mAb-FITC), and it was confirmed that CLIO-CD40 binds to spleen cells as judged from FACS analysis.

In light of the previously described data of unspecific uptake of CLIO by murine endothelial cells it was important to demonstrate the specificity of the CLIO-antibody conjugates. This was achieved by testing the binding in control cells that do not express antigens and by comparison with a matched unspecific rIgG2a antibody. Unstimulated bEnd.3 (CD40-, CD62E-negative) failed to bind the corresponding antibody conjugates. Analogous nanoparticles with rat IgG2a substituted for monoclonal antibodies were used as controls for non-specific labeling. In addition, the binding of the stimulated cells to free antibodies was performed in positive controls. These data show the specific receptor-mediated binding of the conjugates to the corresponding antigen-expressing cells.

Tsourkas et al. have demonstrated that CLIO nanoparticles labeled with the near-infrared fluorochrome Cy5.5 and conjugated to anti-VCAM-1 antibodies or a VCAM-

binding peptide can be used to specifically detect VCAM-1 expression in murine heart endothelial cells and murine dermal endothelial cells by fluorescence and magnetic resonance (¹⁸).

Cell-type-specific targeting by anti-CD3-conjugated nanoparticles of CD3-positive human T-cell leukemia cells and primary T-lymphocytes was observed by Dinauer N (⁸⁴). In this study incubation periods of 4 hours were used, leading to unspecific cellular uptake and internalization of antibody-conjugated nanoparticles into cells. Since their aim was the development of drug carriers selective for cells expressing the CD3 antigen, i.e. cells of the T-lymphocytic lineage, the longer incubation periods were necessary. In contrast, we used a short incubation time (30 minutes) at 5°C in our experiments to reduce unspecific binding of CLIO-conjugates.

5 Summary

The aim of this work was to evaluate the biological properties of one citrate-coated and two different dextran-coated paramagnetic particles with comparable size (iron core 4-10 nm).

Endothelial cells from humans and mice as well as human macrophages were incubated for different time intervals with different particle suspensions. The cellular uptake was semi-quantitatively measured using Prussian blue staining and, in addition, by cellular iron content. Furthermore, the effect of known inhibitors of endocytosis was evaluated. In addition, it was evaluated whether linking of monoclonal antibodies to dextran-coated particles can make them bind specifically to certain cell surface structures.

In conclusion, it was shown that the bEnd.3 cell line, human umbilical vein endothelial cells (HUVECs) and THP-1/macrophage cell lines internalize paramagnetic particles. The ranking of cellular uptake was: VSOP > CMD-coated particles >> CLIO. The different surface coating can influence not only the quantity of the internalization, but also the pathway of internalization.

The binding of antibody-conjugated CLIO to the antigen-expressing cells was specific, with an affinity similar to that of the free antibody. Thus, it seems feasible to use antibody linked SPIOs for molecular imaging.

6 Abbreviations

CD	Cluster designation
CO ₂	Carbon dioxide
CLIO	Crosslinked iron oxide particles
DMEM	Dulbecco's modified Eagle's medium
EDTA	Ethylenediaminetetraacetic acid
ELISA	Enzyme linked immuno sorbent assay
FACS	Fluorescence activated cell scanning
FCS	Fetal calf serum
FITC	Flourescein isothiocyanate
FGF α	Fibroblast growth factor- α
HEPES	Hydroxyethylpiperazine ethane sulfonic acid
HUVEC	Human umbilical vein endothelial cell
IL	Interleukin
INF γ	Interferon gamma
mAB	Monoclonal antibody
MPS	Mononuclear phagocytic system
MRI	Magnetic resonance imaging
LPS	Lipopolysaccharide
PBS	Phosphate buffered saline
PE	Phycoerythrin
PMA	Phorbol-12-myristate-13-acetate
SDS	Sodium dodecyl sulfate
SPIO	Superparamagnitic iron oxide
TNF- α	Tumor necrosis factor- α

7 References

1. Bulte JW, Kraitchman DL. Iron oxide MR contrast agents for molecular and cellular imaging. *NMR Biomed.* 2004;17:484-499.
2. Zhao M, Beauregard DA, Loizou L et al. Non-invasive detection of apoptosis using magnetic resonance imaging and a targeted contrast agent. *Nat Med.* 2001;7:1241-1244.
3. Wang YX, Hussain SM, Krestin GP. Superparamagnetic iron oxide contrast agents: physicochemical characteristics and applications in MR imaging. *Eur Radiol.* 2001;11:2319-2331.
4. Ye Q, Yang D, Williams M et al. In vivo detection of acute rat renal allograft rejection by MRI with USPIO particles. *Kidney Int.* 2002;61:1124-1135.
5. Dousset V, Delalande C, Ballarino L et al. In vivo macrophage activity imaging in the central nervous system detected by magnetic resonance. *Magn Reson Med.* 1999;41:329-333.
6. Weissleder R, Mahmood U. Molecular imaging. *Radiology.* 2001;219:316-333.
7. Weissleder R, Moore A, Mahmood U et al. In vivo magnetic resonance imaging of transgene expression. *Nat Med.* 2000;6:351-355.
8. Herschman HR. Molecular imaging: looking at problems, seeing solutions. *Science.* 2003;302:605-608.
9. Taupitz M, Schmitz S, Hamm B. [Superparamagnetic iron oxide particles: current state and future development]. *Rofo.* 2003;175:752-765.
10. Weissleder R, Elizondo G, Wittenberg J et al. Ultrasmall superparamagnetic iron oxide: characterization of a new class of contrast agents for MR imaging. *Radiology.* 1990;175:489-493.
11. Gupta AK, Gupta M. Synthesis and surface engineering of iron oxide nanoparticles for biomedical applications. *Biomaterials.* 2005;26:3995-4021.
12. Massia SP, Stark J, Letbetter DS. Surface-immobilized dextran limits cell adhesion and spreading. *Biomaterials.* 2000;21:2253-2261.
13. Li JK, Wang N, Wu XS. A novel biodegradable system based on gelatin nanoparticles and poly(lactic-co-glycolic acid) microspheres for protein and peptide drug delivery. *J Pharm Sci.* 1997;86:891-895.
14. Koch AM, Reynolds F, Merkle HP et al. Transport of surface-modified

nanoparticles through cell monolayers. *Chembiochem*. 2005;6:337-345.

15. Jaffe EA, Nachman RL, Becker CG et al. Culture of human endothelial cells derived from umbilical veins. Identification by morphologic and immunologic criteria. *J Clin Invest*. 1973;52:2745-2756.
16. Gräfe M, Bossaller C, Graf K et al. Effect of angiotensin converting enzyme inhibition on bradykinin metabolism of vascular endothelial cells. *Am J Physiol*. 1993;264:H1494-H1497.
17. Marin V, Kaplanski G, Gres S et al. Endothelial cell culture: protocol to obtain and cultivate human umbilical endothelial cells. *J Immunol Methods*. 2001;254:183-190.
18. Tsourkas A, Shinde-Patil VR, Kelly KA et al. In vivo imaging of activated endothelium using an anti-VCAM-1 magneto-optical probe. *Bioconjug Chem*. 2005;16:576-581.
19. Tsuchiya S, Kobayashi Y, Goto Y et al. Induction of maturation in cultured human monocytic leukemia cells by a phorbol diester. *Cancer Res*. 1982;42:1530-1536.
20. Zychlinsky A, Sansonetti P. Perspectives series: host/pathogen interactions. Apoptosis in bacterial pathogenesis. *J Clin Invest*. 1997;100:493-495.
21. Pober JS, Cotran RS. Cytokines and endothelial cell biology. *Physiol Rev*. 1990;70:427-451.
22. Mach F, Schönbeck U, Sukhova GK et al. Reduction of atherosclerosis in mice by inhibition of CD40 signalling. *Nature*. 1998;394:200-203.
23. Lutgens E, Cleutjens KB, Heeneman S et al. Both early and delayed anti-CD40L antibody treatment induces a stable plaque phenotype. *Proc Natl Acad Sci U S A*. 2000;97:7464-7469.
24. Büchner K, Henn V, Gräfe M et al. CD40 ligand is selectively expressed on CD4+ T cells and platelets: implications for CD40-CD40L signalling in atherosclerosis. *J Pathol*. 2003;201:288-295.
25. Bruemmer D, Riggers U, Holzmeister J et al. Expression of CD40 in vascular smooth muscle cells and macrophages is associated with early development of human atherosclerotic lesions. *Am J Cardiol*. 2001;87:21-27.
26. Aukrust P, Muller F, Ueland T et al. Enhanced levels of soluble and membrane-bound CD40 ligand in patients with unstable angina. Possible reflection of T lymphocyte and platelet involvement in the pathogenesis of acute coronary syndromes. *Circulation*. 1999;100:614-620.
27. Schonbeck U, Varo N, Libby P et al. Soluble CD40L and cardiovascular risk in women. *Circulation*. 2001;104:2266-2268.

28. Bevilacqua MP, Pober JS, Mendrick DL et al. Identification of an inducible endothelial-leukocyte adhesion molecule. *Proc Natl Acad Sci USA*. 1987;84:9238-9242.
29. Vestweber D, Blanks JE. Mechanisms that regulate the function of the selectins and their ligands. *Physiol Rev*. 1999;79:181-213.
30. Bevilacqua MP, Stengelin S, Gimbrone MA, Jr. et al. Endothelial leukocyte adhesion molecule 1: an inducible receptor for neutrophils related to complement regulatory proteins and lectins. *Science*. 1989;243:1160-1165.
31. Vestweber D. The selectins and their ligands. *Curr Top Microbiol Immunol*. 1993;184:65-75.
32. Van der Wal AC, Das PK, Tigges AJ et al. Adhesion molecules on the endothelium and mononuclear cells in human atherosclerotic lesions. *Am J Pathol*. 1992;141:1427-1433.
33. O'Brian KD, McDonald TO, Chait A et al. Neovascular expression of E-selectin, intercellular adhesion molecule-1, and vascular cell adhesion molecule-1 in human atherosclerosis and their relation to intimal leukocyte content. *Circulation*. 1996;93:672-682.
34. Dong ZM, Chapman SM, Brown AA et al. The combined role of P- and E-selectins in atherosclerosis. *J Clin Invest*. 1998;102:145-152.
35. Gräfe M, Zakrzewicz A, Graf K et al. Menschliche kardiale mikro- und makrovaskuläre Endothelzellen zeigen ein unterschiedliches Expressionsmuster von Adhäsionsmolekülen und reagieren unterschiedlich auf oxidierte LDL. *Z Kardiol*. 1999;88:828-837.
36. Gräfe M, Auch-Schwelk W, Zakrzewicz A et al. Angiotensin II induced leukocyte adhesion on human coronary endothelial cells is mediated by E-selectin. *Circ Res*. 1997;81:804-811.
37. Libby P. Inflammation in atherosclerosis. *Nature*. 2002;420:868-874.
38. Montesano R, Pepper MS, Mohle-Steinlein U et al. Increased proteolytic activity is responsible for the aberrant morphogenetic behavior of endothelial cells expressing the middle T oncogene. *Cell*. 1990;62:435-445.
39. Yao L, Setiadi H, Xia L et al. Divergent inducible expression of P-selectin and E-selectin in mice and primates. *Blood*. 1999;94:3820-3828.
40. Omid Y, Campbell L, Barar J et al. Evaluation of the immortalised mouse brain capillary endothelial cell line, b.End3, as an in vitro blood-brain barrier model for drug uptake and transport studies. *Brain Res*. 2003;990:95-112.
41. Stawowy P, Meyborg H, Stibenz D et al. Furin-like proprotein convertases are

central regulators of the membrane type matrix metalloproteinase-pro-matrix metalloproteinase-2 proteolytic cascade in atherosclerosis. *Circulation*. 2005;111:2820-2827.

42. Gräfe M, Steinheider G, Desaga U et al. Characterization of two distinct mechanisms for induction of apoptosis in human vascular endothelial cells. *Clin Chem Lab Med*. 1999;37:505-510.
43. Wyllie AH, Morris RG, Smith AL et al. Chromatin cleavage in apoptosis: association with condensed chromatin morphology and dependence on macromolecular synthesis. *J Pathol*. 1984;142:67-77.
44. Bacon BR, Stark DD, Park CH et al. Ferrite particles: a new magnetic resonance imaging contrast agent. Lack of acute or chronic hepatotoxicity after intravenous administration. *J Lab Clin Med*. 1987;110:164-171.
45. Stark DD, Weissleder R, Elizondo G et al. Superparamagnetic iron oxide: clinical application as a contrast agent for MR imaging of the liver. *Radiology*. 1988;168:297-301.
46. Harisinghani MG, Barentsz J, Hahn PF et al. Noninvasive detection of clinically occult lymph-node metastases in prostate cancer. *N Engl J Med*. 2003;348:2491-2499.
47. Anzai Y, Brunberg JA, Lufkin RB. Imaging of nodal metastases in the head and neck. *J Magn Reson Imaging*. 1997;7:774-783.
48. Ruehm SG, Corot C, Vogt P et al. Magnetic resonance imaging of atherosclerotic plaque with ultrasmall superparamagnetic particles of iron oxide in hyperlipidemic rabbits. *Circulation*. 2001;103:415-422.
49. Sayegh Y, Pochon S, Vallee JP et al. Detection of experimental hepatic tumors using long circulating superparamagnetic particles. *Invest Radiol*. 2001;36:15-21.
50. Knollmann FD, Bock JC, Rautenberg K et al. Differences in predominant enhancement mechanisms of superparamagnetic iron oxide and ultrasmall superparamagnetic iron oxide for contrast-enhanced portal magnetic resonance angiography. Preliminary results of an animal study original investigation. *Invest Radiol*. 1998;33:637-643.
51. Saeed M, Wendland MF, Engelbrecht M et al. Value of blood pool contrast agents in magnetic resonance angiography of the pelvis and lower extremities. *Eur Radiol*. 1998;8:1047-1053.
52. Wagner S, Schnorr J, Pilgrimm H et al. Monomer-coated very small superparamagnetic iron oxide particles as contrast medium for magnetic resonance imaging: preclinical in vivo characterization. *Invest Radiol*. 2002;37:167-177.

53. McLachlan SJ, Francisco JC, Pernicone JR et al. Efficacy evaluation of gadoteridol for MR angiography of intracranial vascular lesions. *J Magn Reson Imaging*. 1994;4:405-411.
54. McLachlan SJ, Morris MR, Lucas MA et al. Phase I clinical evaluation of a new iron oxide MR contrast agent. *J Magn Reson Imaging*. 1994;4:301-307.
55. Chouly C, Pouliquen D, Lucet I et al. Development of superparamagnetic nanoparticles for MRI: effect of particle size, charge and surface nature on biodistribution. *J Microencapsul*. 1996;13:245-255.
56. Yeh TC, Zhang W, Ildstad ST et al. In vivo dynamic MRI tracking of rat T-cells labeled with superparamagnetic iron-oxide particles. *Magn Reson Med*. 1995;33:200-208.
57. Weissleder R, Cheng HC, Bogdanova A et al. Magnetically labeled cells can be detected by MR imaging. *J Magn Reson Imaging*. 1997;7:258-263.
58. Schoepf U, Marecos EM, Melder RJ et al. Intracellular magnetic labeling of lymphocytes for in vivo trafficking studies. *Biotechniques*. 1998;24:642-651.
59. Josephson L, Tung CH, Moore A et al. High-efficiency intracellular magnetic labeling with novel superparamagnetic-Tat peptide conjugates. *Bioconjug Chem*. 1999;10:186-191.
60. Kelly KA, Allport JR, Tsourkas A et al. Detection of vascular adhesion molecule-1 expression using a novel multimodal nanoparticle. *Circ Res*. 2005;96:327-336.
61. Kang HW, Josephson L, Petrovsky A et al. Magnetic resonance imaging of inducible E-selectin expression in human endothelial cell culture. *Bioconjug Chem*. 2002;13:122-127.
62. Fleige G, Seeberger F, Laux D et al. In vitro characterization of two different ultrasmall iron oxide particles for magnetic resonance cell tracking. *Invest Radiol*. 2002;37:482-488.
63. Davda J, Labhassetwar V. Characterization of nanoparticle uptake by endothelial cells. *Int J Pharm*. 2002;233:51-59.
64. Liu SM, Magnusson KE, Sundqvist T. Microtubules are involved in transport of macromolecules by vesicles in cultured bovine aortic endothelial cells. *J Cell Physiol*. 1993;156:311-316.
65. Lee JS, Gotlieb AI. Microtubules regulate aortic endothelial cell actin microfilament reorganization in intact and repairing monolayers. *Histol Histopathol*. 2005;20:455-465.
66. Fleige G, Seeberger F, Laux D et al. In vitro characterization of two different ultrasmall iron oxide particles for magnetic resonance cell tracking. *Invest Radiol*.

2002;37:482-488.

67. Davies P, Allison AC. Effects of cytochalasin B on endocytosis and exocytosis. *Front Biol.* 1978;46:143-160.
68. Moore A, Weissleder R, Bogdanov A, Jr. Uptake of dextran-coated monocrystalline iron oxides in tumor cells and macrophages. *J Magn Reson Imaging.* 1997;7:1140-1145.
69. Rogers WJ, Basu P. Factors regulating macrophage endocytosis of nanoparticles: implications for targeted magnetic resonance plaque imaging. *Atherosclerosis.* 2005;178:67-73.
70. West MA, Antoniou AN, Prescott AR et al. Membrane ruffling, macropinocytosis and antigen presentation in the absence of gelsolin in murine dendritic cells. *Eur J Immunol.* 1999;29:3450-3455.
71. Sundstrom JB, Mao H, Santoianni R et al. Magnetic resonance imaging of activated proliferating rhesus macaque T cells labeled with superparamagnetic monocrystalline iron oxide nanoparticles. *J Acquir Immune Defic Syndr.* 2004;35:9-21.
72. Qaddoumi MG, Ueda H, Yang J et al. The characteristics and mechanisms of uptake of PLGA nanoparticles in rabbit conjunctival epithelial cell layers. *Pharm Res.* 2004;21:641-648.
73. Matuszewski L, Persigehl T, Wall A et al. Cell tagging with clinically approved iron oxides: feasibility and effect of lipofection, particle size, and surface coating on labeling efficiency. *Radiology.* 2005;235:155-161.
74. Seymour L, Schacht E, Duncan R. The effect of size of polystyrene particles on their retention within the rat peritoneal compartment, and on their interaction with rat peritoneal macrophages in vitro. *Cell Biol Int Rep.* 1991;15:277-286.
75. Ishikawa Y, Muramatsu N, Ohshima H et al. Effect of particle size on phagocytosis of latex particles by guinea-pig polymorphonuclear leucocytes. *J Biomater Sci Polym Ed.* 1991;2:53-60.
76. Berry CC, Wells S, Charles S et al. Dextran and albumin derivatised iron oxide nanoparticles: influence on fibroblasts in vitro. *Biomaterials.* 2003;24:4551-4557.
77. Perez JM, Josephson L, O'loughlin T et al. Magnetic relaxation switches capable of sensing molecular interactions. *Nat Biotechnol.* 2002;20:816-820.
78. Weissleder R, Ntziachristos V. Shedding light onto live molecular targets. *Nat Med.* 2003;9:123-128.
79. Frias JC, Williams KJ, Fisher EA et al. Recombinant HDL-like nanoparticles: a specific contrast agent for MRI of atherosclerotic plaques. *J Am Chem Soc.*

2004;126:16316-16317.

80. Winter PM, Morawski AM, Caruthers SD et al. Molecular imaging of angiogenesis in early-stage atherosclerosis with alpha(v)beta3-integrin-targeted nanoparticles. *Circulation*. 2003;108:2270-2274.
81. Ramos CL, Kunkel EJ, Lawrence MB et al. Differential effect of E-selectin antibodies on neutrophil rolling and recruitment to inflammatory sites. *Blood*. 1997;89:3009-3018.
82. Malek NP, Pluemp J, Kubicka S et al. Molecular mechanisms of TNF receptor-mediated signaling. *Recent Results Cancer Res*. 1998;147:97-106.
83. Azzawi M, Hasleton P. Tumour necrosis factor alpha and the cardiovascular system: its role in cardiac allograft rejection and heart disease. *Cardiovasc Res*. 1999;43:850-859.
84. Dinauer N, Balthasar S, Weber C et al. Selective targeting of antibody-conjugated nanoparticles to leukemic cells and primary T-lymphocytes. *Biomaterials*. 2005;26:5898-5906.

8 Anhang

8.1 Danksagung

Mein Dank gilt vor allem:

PD Dr. med. Michael Gräfe für die herausragende Betreuung und seine Unterstützung während aller Phasen der Erstellung dieser Arbeit.

Prof. Dr. Eckart Fleck für die Überlassung des Themas und die Unterstützung bei der Erstellung dieser Arbeit.

Prof. Dr. Kristof Graf, Dipl. Ing Heike Meyborg, Frau K. Atrott, Frau C. Hänsch, Ph. D. Thore Dietrich und allen anderen Mitgliedern der Arbeitsgruppe für Experimentelle Kardiologie am Deutschen Herzzentrum Berlin.

PD Dr. Dietger Stibenz für die stets gute Zusammenarbeit und die Hilfe bei der Versuchsanordnung.

Meinen Eltern und Prof. Dr. Y. Weng für ihre Unterstützung während der Promotion.

8.2 Eidesstattliche Erklärung

Ich erkläre, die vorliegende Dissertationsschrift ohne fremde Hilfe verfasst zu haben. Die beschriebenen Ergebnisse sind selbst gewonnen. Die verwendeten Hilfsmittel, die Zusammenarbeit mit anderen Wissenschaftlern sowie die Literatur wurden vollständig angegeben. Ohne die Hilfe Dritter verfasst und auch in Teilen keine Kopie anderer Arbeiten dargestellt habe.

Berlin, 25. 12. 2005

Zhi Yu

8.3 **Lebenslauf** (Seit 56/57)

Aus Datenschutzgründen wird mein Lebenslauf im Netz nicht veröffentlicht.